GEORGIA DOT RESEARCH PROJECT 17-12

FINAL REPORT

MECHANICAL INTEGRITY AND SUSTAINABILITY OF PRE-STRESSED CONCRETE BRIDGE GIRDERS REPAIRED BY EPOXY INJECTION – PHASE III

OFFICE OF PERFORMANCE-BASED MANAGEMENT AND RESEARCH
15 KENNEDY DRIVE
FOREST PARK, GA 30297-2534

TECHNICAL REPORT DOCUMENTATION PAGE

1. Report No.: FHWA-GA-19-1712	2. Government Accession No.:	3. Recipient's Catalog No.:

4. Title and Subtitle: Mechanical integrity and sustainability of pre-stressed concrete bridge girders repaired by epoxy injection - Phase III	5. Report Date: February 2019
	6. Performing Organization Code:
7. Author(s): C.F. Arson, L.K. Stewart, N. Gao	8. Performing Organ. Report No.: 17-12
9. Performing Organization Name and Address: Georgia Institute of Technology, School of Civil and Environmental Engineering, 790 Atlantic Drive NW, Atlanta, GA 30332	10. Work Unit No.:
	11. Contract or Grant No.: 0015304
12. Sponsoring Agency Name and Address: Georgia Department of Transportation, Office of Performance-based Management and Research, 15 Kennedy Drive, Forest Park, GA 30297-2534	13. Type of Report and Period Covered: Final; August 2017 – February 2019
	14. Sponsoring Agency Code:
15. Supplementary Notes:	

16. Abstract: During pre-stress transfer, the bottom portion of steel-reinforced concrete girders is subjected to an important compression induced by the relaxation of tension in the bars, which opens longitudinal cracks along the horizontal axis. Reactions at the supports induce shear stress, which sometimes translates into additional diagonal cracks at the ends of the girders. During the subsequent lifespan of the girder, a variety of crack patterns can occur, including longitudinal (along the beam axis), transverse (perpendicular to the beam axis), and diagonal cracks. At present, there is a need to assess the mechanical integrity and sustainability of pre-stressed concrete beams during the entire life cycle of the built infrastructure, which includes crack propagation, crack reparation, and repaired crack aging with possible re-opening. As such, this three-phase research program seeks to develop modeling strategies to predict the behavior of cracked concrete repaired by epoxy. The subject of this technical report is the Phase III research effort, which includes the experimental characterization of materials and systems for the computational (Phase I and Phase II) model calibration and validation. Three main sets of experiments were conducted: (1) concrete and epoxy-repaired concrete cylinders in uniaxial compression and splitting tension, (2) mortar cylinders in uniaxial compression and splitting tension, and (3) “as-built” and epoxy-repaired concrete beams via three-point bending.

17. Key Words: Pre-stressed concrete, epoxy, repair	18. Distribution Statement:		
19. Security Class (this report): Unclassified	20. Security Class (this page): Unclassified	21. Number of Pages: 67	22. Price:

Form DOT 1700.7 (8-69)

GDOT Research Project 17-02

Final Report

MECHANICAL INTEGRITY AND SUSTAINABILITY OF PRE-STRESSED CONCRETE BRIDGE GIRDERS REPAIRED BY EPOXY INJECTION – PHASE III

By

Lauren Stewart, Assistant Professor

Nan Gao, Research Engineer

Chloe Arson, Associate Professor

Georgia Tech Research Corporation
Atlanta, Georgia

Contract with

Georgia Department of Transportation

In cooperation with

U.S. Department of Transportation
Federal Highway Administration

February 4, 2019

TABLE OF CONTENTS

Page

LIST OF TABLES

Page

LIST OF FIGURES

Page

EXECUTIVE SUMMARY

During pre-stress transfer, the bottom portion of steel-reinforced concrete girders is subjected to an important compression induced by the relaxation of tension in the bars, which opens longitudinal cracks along the horizontal axis. Reactions at the supports induce shear stress, which sometimes translates into additional diagonal cracking at the ends of the girders. During the subsequent lifespan of the girder, a variety of crack patterns can occur, including longitudinal (along the beam axis), transverse (perpendicular to the beam axis), and diagonal cracks. At present, there is a need to assess the mechanical integrity and sustainability of pre-stressed concrete beams during the entire life cycle of the built infrastructure, which includes crack propagation, crack reparation, and repaired crack aging with possible re-opening. As such, this three-phase research program seeks to develop modeling strategies to predict the behavior of cracked concrete repaired by epoxy.

The subject of this technical report is the Phase III research effort, which includes the experimental characterization of materials and systems for the computational (Phases I and II) model calibration and validation. Three main sets of experiments were conducted on (1) concrete and epoxy-repaired concrete cylinders, (2) mortar cylinders, and (3) concrete beams.

The concrete and epoxy-repaired cylinder experiments consisted of both uniaxial and splitting tension tests and involved a newly developed protocol for including epoxy repair into these material characterization tests. The mortar cylinder experiments also consisted of uniaxial and splitting tension characterization. Additionally, a study as to the effect of specimen size for computational efficiency was conducted.

Both unreinforced and reinforced concrete beams were tested using a three-point bending procedure. In both cases, both "as-built" and epoxy-repaired specimens were tested for comparison and for model validation. The epoxy-repaired reinforced specimens were loaded to induce cracking of various levels, unloaded, repaired with epoxy, and reloaded to failure. In the cases where the cracks were very small (< 0.006 in), the epoxy did not have a significant effect on the ultimate capacity, but the beam behaved in a more brittle fashion. Interestingly, in the experiments where the cracks were larger (> 0.006 in), the beams exhibited a much higher capacity than the "as-built" and the failure mechanism and ductility of the beam was affected. Because of this, further research could be conducted to better understand the overall effect that epoxy has on larger pre-stressed beams and, subsequently, the effect on the entire bridge structure including loads transferred to adjacent elements.

ACKNOWLEDGEMENTS

The following individuals at GDOT provided many valuable suggestions throughout this study: Mr. Christopher Watson, Mr. Jon Smith, Dr. Peter Wu, and Mr. David Jared.

The opinions and conclusions expressed herein are those of the authors and do not represent the opinions, conclusions, policies, standards, or specifications of GDOT or of other cooperating organizations.

The experimental research described herein was performed at the Georgia Institute of Technology Structural Engineering and Materials Laboratory (SEML). Mr. Jeremy Mitchell, SEML Facilities Manager, and Graduate Students, Rebecca Tien, Pei Wang, and Koochul Ji, facilitated the setup and completion of the testing.

The authors express their profound gratitude to all of these individuals for their assistance and support during the completion of this research project.

CHAPTER 1. INTRODUCTION AND BACKGROUND

1.1 Introduction

During pre-stress transfer, the bottom portion of steel-reinforced concrete girders is subjected to an important compression induced by the relaxation of tension in the bars, which opens longitudinal cracks along the horizontal axis. Reactions at the supports induce shear stress, which sometimes leads to the formation of additional diagonal cracks at the ends of the girders. During the subsequent lifespan of the girder, a variety of crack patterns can occur, including longitudinal (along the beam axis), transverse (perpendicular to the beam axis), and diagonal cracks. When cracks occur, the National Cooperative Highway Research Program (NCHRP) recommends as follows (Tadros et al., 2010): accept the girders if longitudinal cracks are less than 0.012 in. wide; apply cementitious packing materials to cracks between 0.012 in. and 0.025 in. wide; inject epoxy in cracks that are 0.025 in. to 0.050 in. wide; and reject the girder and replace the girder if cracks are wider than 0.05 in. Alternatively, the Precast Concrete Institute (PCI) guide (2001) uses three defect categories: those that can be accepted without repair, those that can be repaired, and those that must be rejected. The PCI guide has more detailed trouble shooting and repair procedures, depending on the location, orientation, length and width of the cracks. It specifies a minimum width for epoxy repair beginning at 0.006 inches.

Experimental studies showed that cracked concrete had lower mechanical strength than intact concrete, and that 80% of the lost concrete strength could be recovered by epoxy injection (Issa and Debs, 2007). It has also been shown that epoxy injection can increase the fatigue resistance of cracked mortar, but that the mechanical performance of

repaired concrete decreases as temperature increases (Shin et al., 2011). In general, repaired beams exhibit a more brittle behavior than intact or corroded beams (Okada et al., 1988). According to the literature review completed in Phase I of this project, the model proposed by L. Bardella (2001) properly describes the nonlinear viscoelastic behavior of epoxy resins in the glassy state. However, no model has ever been proposed to predict the behavior of cracked concrete repaired by epoxy. At present, there is a need to assess the mechanical integrity and sustainability of pre-stressed concrete beams during the entire life cycle of the built infrastructure, which includes crack propagation, crack reparation, and repaired crack aging with possible re-opening.

1.2 Prior Phases

In Phase I of the project, the researchers calibrated a Continuum Damage Mechanics model (the Differential Stress-Induced Damage model, DSID) to predict the propagation of cracks in three directions in concrete, according to net tension and compression criteria (Xu and Arson, 2014; Xu et al., 2016). A static load test presented in Tadros et al. (2010) was simulated with ABAQUS Finite Element (FE) software for four types of girders (Tennesse, Florida, Virginia, and Washington State designs), with and without pre-loading damage in the end zone. In order to study vertical cracks, horizontal cracks, diagonal cracks, and cracks on the bottom flange, damage was assigned to end zone elements in designated space directions prior to loading. The DSID model was used to represent concrete and elastic bar elements were used to represent the pre-stressed steel reinforcements. The effect of initial cracks on deflection was minimal; increased displacements were only noted in the area close to the point of application of the clamping force. The most noticeable effects on deflection were obtained for vertical and

diagonal cracks. Note that these results only apply for smeared damage under a moderate static load. Then a portion of typical bridge deck supported by pre-stressed girders was modeled with the FE Method. Beam deflection and concrete damage induced by static loads were calculated with and without diffuse micro-cracking consecutive to pre-stress transfer. Initial damage configurations corresponded to typical crack patterns listed in the PCI bridge repair guidelines. In general, lower stress and higher deflections were found for higher initial damage.

The objective of Phase II, which had an initial portion that occurred in parallel with Phase III, is to simulate localized fracture propagation and epoxy repair in concrete. Researchers modeled mortar and concrete cylinders by using the Discrete Element Method (DEM). Mortar DEM parameters were calibrated against Phase III mortar cylinder tests. Concrete aggregates were then scanned. Point clouds obtained by scanning were imported in MATLAB to reconstruct aggregates' shapes. Aggregate shapes were then generated within the DEM mortar models, in order to match the aggregate size distribution of GDOT concrete. The DEM parameters of the aggregates and of the Interfacial Transition Zone (ITZ) between the aggregates and the mortar were then calibrated against the results of concrete cylinder tests performed in Phase III. DEM analyses allowed understanding the effects of aggregate mechanical properties and of ITZ adhesive properties on fracture propagation and failure mechanisms in the concrete used in GDOT. Notably, it was found that aggregates used in the composition of the concrete act as weak inclusions that decrease concrete strength.

Researchers are now using a cohesive segment model implemented in the eXtended Finite Element Method (XFEM) to simulate fracture propagation in concrete. Initially,

the cohesive model was calibrated against shear and compression test results published in the literature for concrete alone. Parameters were then recalibrated when Phase III results on plain concrete cylinder tests and plain unreinforced concrete three-point bending tests became available. Researchers are now developing a Molecular Dynamics (MD) model to simulate pull out tests conducted on a concrete/epoxy interface. MD results will provide the concrete/epoxy interface energy that will be used in replacement of the concrete fracture energy release rate when switching from plain to repaired concrete in the XFEM model. XFEM simulations of repaired concrete will be compared with the repaired concrete cylinder and beam tests conducted in Phase III for further calibration and validation.

Simulations on pre-stressed concrete beams were then conducted with the XFEM. Steel/concrete interface parameters were calibrated against published experimental and numerical datasets. A damage-plasticity model is now being calibrated to simulate three-point bending tests done in pre-stressed concrete beams before and after reparation. The continuum approach has the advantage to converge more easily and to be faster than the XFEM. The calibration of the continuum damage-plasticity model against the same datasets as those used for the calibration of the XFEM model will allow calculating the geometric properties of fractures from the knowledge of the equivalent continuum damage obtained in the continuum damage-plasticity simulations.

Lastly, pre-stress relaxation and service loads in pre-stressed steel reinforced concrete girders will be simulated before and after epoxy injection to check the girder acceptance criteria recommended by the NCHRP and by the PCI. Girders and bridge scale models proposed in Phase I will be used for both static and dynamic loading, and

the fatigue limit will be determined. In order to assess the stability and sustainability of damaged and repaired PSC girders, life cycles including thermal fluctuations will be simulated. The final product of this Phase II research will be a repair guideline that will help GDOT's engineers and inspectors decide whether defects observed on girders can be accepted, and if not, whether they can be repaired, and by what method.

1.3 Phase III Objectives and Summary

Experimental data on the mechanical properties of cracked concrete repaired by epoxy is scarce. The research objective of Phase III was to develop and conduct experiments to measure the mechanical properties of cracked concrete repaired by epoxy in the laboratory, in order to calibrate and validate the cohesive segment models proposed in Phase II. The Phase III experiments evaluated three specimen types: concrete cylinders, mortar cylinders, and concrete beams. The concrete cylinders were evaluated in both compression and splitting tension and the cylinders were divided into two categories: plain and epoxy-repaired. The mortar cylinders were evaluated in compression and splitting tension. The beams consisted of both unreinforced and reinforced specimens; both "as-built" and epoxy-repaired specimens were experimentally characterized.

1.4 Report Organization

Chapter 2 of this report summarizes the experimental methods, specimens, and results of the concrete cylinder experiments, which were conducted on both plain and epoxy-repaired specimens.

Chapter 3 describes the experimental methods, specimens, and results of the mortar experiments.

Chapter 4 contains the experimental methods, specimens, and results of the beam experiments, which were conducted on both the "as-built" and epoxy-repaired specimens.

Chapter 5 explains the conclusions for Phase III of this research program.

Chapter 6 lists the references cited in this report.

The Appendices contain drawings of the experimental specimens and material information.

CHAPTER 2. CONCRETE CYLINDER EXPERIMENTS

The experiments presented in this chapter are divided into two categories: plain concrete cylinder experiments (Section 2.1) and epoxy-repaired concrete cylinder experiments (Section 2.2).

2.1 Plain Concrete Experiments

The majority of the experiments were performed on cylinders of plain concrete. These experiments were conducted to provide both compressive and tensile data to calibrate the parametes of the plain concrete cohesive segment model.

2.1.1 Specimen Size Selection

Four initial concrete cylinder experiments were conducted to determine the specimen size as well as to refine the experimental protocol. Experiments were conducted in tension via splitting and uniaxial compression. Splitting tension experiments, sometimes referred to as the Brazilian test (see Section 2.1.4), were initially conducted on 4 inch x 8 inch cylinder specimens. The concrete behaved as expected in terms of strength, but upon visual inspection of each specimen after failure, it was noticed that the fracture occurred off-center. A primary crack formed from the side of the bearing strip and a secondary crack formed on the opposite side of the bearing strip, as shown in Figure 1. Evidence from the literature suggests that the cause of the off-center cracking was caused from the ratio of bearing strip width to specimen diameter (Coronado and Lopez, 2008).

The initial tensile splitting tests were also used to verify the ability to capture high speed video of the crack propagation through the face of the sample. These initial tests indicated that the fracture of the 4 inch x 8 inch cylinders happened too quickly for the 1,000 frames per second (fps) high-speed camera to capture quality data. From the literature, it was found that many experiments used 6 inch x 12 inch cylinders to monitor the crack growth with such cameras (Ross et al., 1996; Li, 2004). As a result, it was determined that 6 inch x 12 inch cylinders would be used for for future experiments in the study in order to ensure and monitor symmetric crack propogation.

Figure 1. Undesired tensile splitting failure of initial 4 inch x 8 inch plain concrete specimen.

2.1.2 Materials

The concrete used in these experiments was made by Thomas Concrete and followed the GDOT Specification for pre-stressed concrete (GDOT, 2013). The concrete provided by Thomas Concrete had mixture weight fractions and properties are listed in Table 1. Additional properties that were in the concrete mixture upon arrival are listed in Table 2.

Table 1. Concrete mix used in concrete cylinder experiments.

Material	Weight Fraction
Cement	18.61%
Water	5.28%
Fine Aggregate	28.33%
Course Aggregate	47.77%

Table 2. Properties of concrete used in concrete cylinder experiments

Property	
Water-cement ratio	0.3545
Cement Type	Type I
Slump	3.25 inch
Specific Gravity (Course Aggregate)	2.71
Specific Gravity (Fine Aggregate)	2.69

The composition of the coarse aggregate was granite-gneiss aggregate from Norcross, Georgia, distributed by Vulcan Materials Company. The coarse aggregate used was size 67. The granite-gneiss aggregates are formed as a banded combination of an igneous rock (granite) and its metamorphic rock counterpart in gneiss. Both rocks are primarily composed of strained and microcrystalline quartz. Given these various component parts, the rocks are susceptible to alkali-silica reaction (ASR), which can cause microcracks in the concrete due to expansion of the ASR gel with water (Alexander and Mindess, 2014). For the purpose of this research, it was determined that the effect of ASR gel on crack propagation could be ignored.

Granite-Gneiss aggregates, as shown in Figure 2, can be classified as having a surface texture a crystalline, a sub-angular shape, and a low sphericity. Coarse aggregates' texture and shape can affect the presence of stress concentrations and the overal fracture mechanisms of the concrete. Therefore, scans of individual aggregate were conducted to create realistic and precise aggregate shapes for the Phase II models in

order to facilitate more accurate prediction of the location and timing of microcracking. A *Matter and Form 3D Tabletop Scanner*, as shown in Figure 3, was used to create three-dimensional point cloud files to generate realistic shapes of aggregate within the model. Examples of the point cloud aggregate scans from this research are shown in Figure 4.

Figure 2. Granite-Gneiss aggregate used in concrete cylinder mix.

Figure 3. Matter and Form 3D Tabletop Scanner used for developing realistic aggregate models.

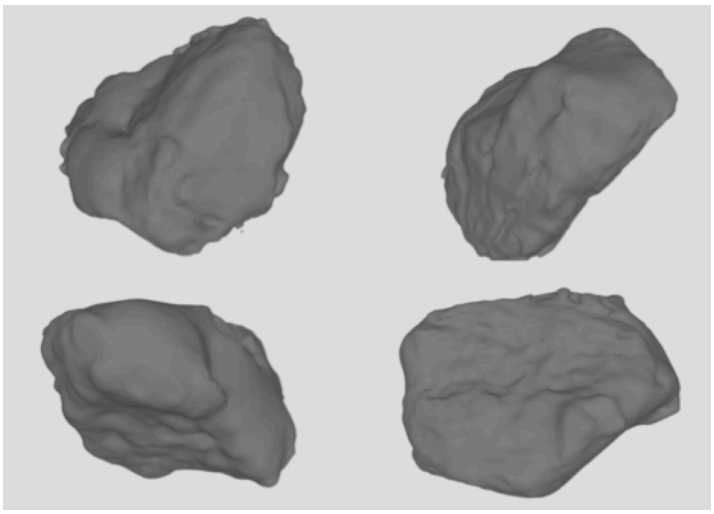

Figure 4. Point cloud renderings from aggregate scans.

2.1.3 Uniaxial Compression Experiments

To understand and quantify the compressive behavior of plain concrete, a uniaxial compression experiment was used. In this experiment, compressive strength can be found by uniformly loading a sample axially until failure. The strength is defined as the ultimate compression load per cross-sectional area. Compressive strength is typically obtained using cubical or cylindrical samples. Cubical specimens are prevalent in Europe while cylindrical samples are standard in the United States, Canada, and Australia. The standard cylinder size is 6 inch x 12 inch, although other sizes are permitted. This research used ASTM C39 procedures to determine the compressive behaviour of plain concrete. The SATEC PRISM MKIII-C machine with INSTRON 59-R7 controller located at the Georgia Institute of Technology Structural Engineering and Materials Laboratory was used to conduct the uniaxial compression experiments. The experiments were conducted with a loading rate of 60 kips per minute. An example of the test setup is shown in Figure 5. When loaded in uniaxial compression following ASTM C39, concrete typically fails in one of the six fracture patterns; these patterns are illustrated in Figure 6.

The plain concrete cylinder experiments are categorized in two groups. Group 1 includes concrete samples that were cured and aged in a controlled fog room environment for the duration of their sample age. Group 2 includes samples that were removed from the controlled environment at 56 days and were then allowed to age at ambient lab temperatures until their test date. Group 2 cylinders are the concrete cylinder samples used to determine the compressive strength of the concrete used for the beams tested (see Chapter 4). Therefore, these cylinders were removed from the controlled environment of the fog room in order to have the same aging environment and moisture content as those of the beams that were removed from the fog room at 56 days for storage. The compressive strengths of the cylinders are reported in *Table 3*. Figure 7 shows the data graphically by group.

Figure 5. Uniaxial compression setup as outlined in ASTM C39.

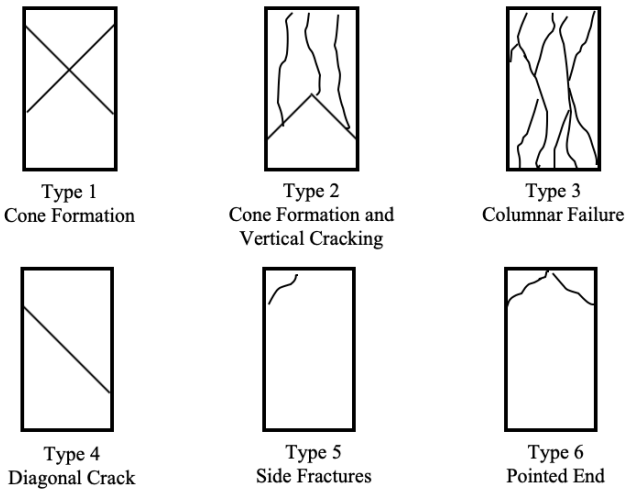

Figure 6. Schematics of typical uniaxial compression fracture patterns (ASTM, 2018).

Table 3. Summary of plain concrete cylinder average compressive strengths.

Sample Age (days)	Compressive Strength, f'c (ksi)	Group Category
28	4.72	1
49	4.68	1
74	5.17	2
95	5.13	2
104	5.03	2
112	5.13	2
119	5.06	2
133	5.66	2

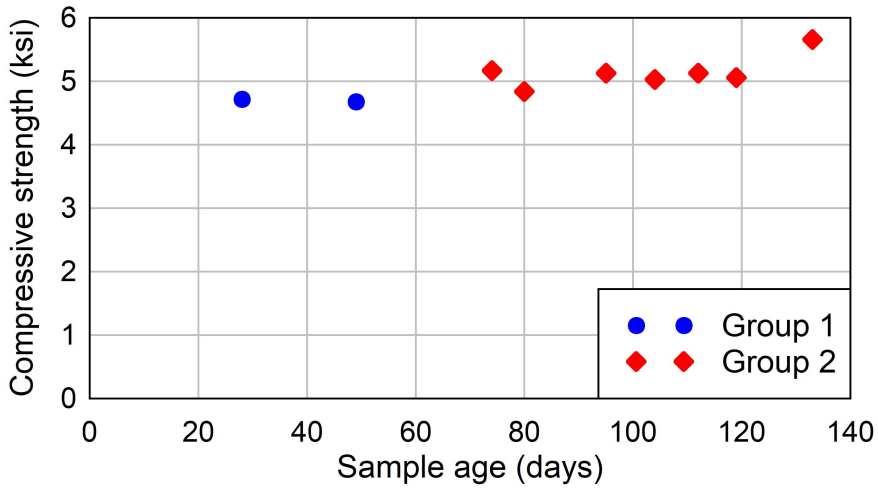

Figure 7. Concrete cylinder average compressive strength at different ages.

As discussed previously, the compressive strengths of the plain concrete cylinders were determined using ASTM C39 procedures. However, since the Group 2 samples were not at the standard moisture content of Saturated Surface Dry (SSD), a slightly modified ASTM C39 procedure was used. This modification allowed for a lower-than-standard moisture content of the concrete cylinders in order to remain consistent with the beam experiments, which are presented in Chapter 4. Figure 8 illustrates the differences between the compressive stress-strain curves of the Group 1 and Group 2 samples. The Group 1 samples demonstrated a higher modulus of elasticity than the Group 2 samples. This difference is consistent with the literature (Reinhardt et al., 1990) that states that concrete with a higher moisture content can exhibit higher modulus as the moisture increases the stiffness of the concrete. The difference in compressive strength between Group 1 and Group 2 cylinders can also be attributed to the difference in sample age between the groups. All Group 2 samples were older than all Group 1 cylinders.

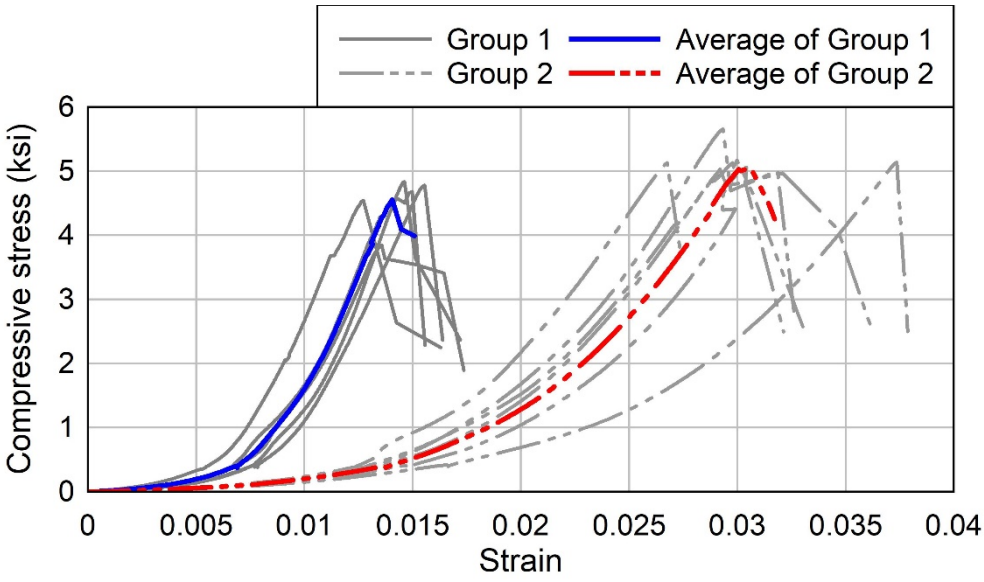

Figure 8. Compressive test results of plain 6 inch x 12 inch concrete cylinders.

Although the two groups exhibited different stress-strain behaviors, both groups had similar failure modes. Utilizing the classifications given in Figure 6, the cylinders primarily demonstrated a columnar failure mode. A posttest photo showing the failure from an example experiment is given in Figure 9.

Figure 9. Typical plain concrete behavior indicative of a type 3 columnar failure.

2.1.4 Splitting Tension Experiments

One of the most widely used methods to determine the tensile strength of concrete is the split cylinder test, sometimes known as the Brazilian test or Splitting Tension test. The split cylinder test was developed by Professor Fernando L.L.B Carneiro and presented at the 5th meeting of the Brazilian Association for Technical Rules in 1943 (Monteiro, 2006). The experiment involves applying a vertical compressive force perpendicular to the cylindrical axis of the sample. The load is increased until the cylinder ruptures. Figure 10 illustrates the test set up and schematics of the split cylinder

test. The methodology and procedures of the test followed in this research were that of ASTM C496 (ASTM, 2017).

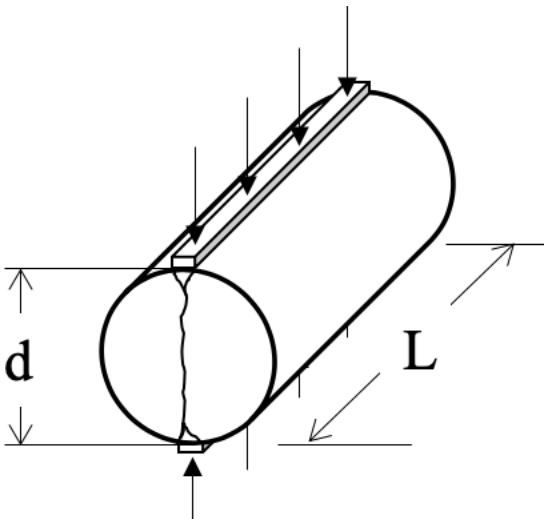

Figure 10. Splitting tension test schematic.

From this setup, the tensile strength is thus assumed to be governed by linearly elastic behavior as stated in Equation 1

$$f_{st} = \frac{2P}{\pi L d} \qquad \text{Equation 1}$$

where f_{st} is the ultimate splitting tensile strength, P is the maximum applied load as indicated by the testing machine, L is the length of the cylinder, and d is the diameter. For this research, the SATEC PRISM MKIII-C with INSTRON 59-R7 controller located at the Georgia Institute of Technology Structural Engineering and Materials Laboratory was used to load at 11.3 kips per minute. The experimental setup is shown in Figure 11.

Figure 11. Splitting tension experimental setup.

The splitting tension cylinder samples were categorized in the same two groupings as the uniaxial compression test sample groupings: Group 1 is included concrete samples that were cured and aged in a controlled fog room environment for the duration of their sample age, while Group 2 included samples that were removed from the controlled environment at 56 days and allowed to age at ambient lab temperatures until their test date. As previously stated, Group 2 cylinders are the concrete cylinder samples used to determine the corresponding splitting tensile strength of the concrete used in the beams tested (see Chapter 4). Therefore, these cylinders were removed from the controlled environment of the fog room to have the same aging environment and moisture content as those of the beams, which were removed from the fog room at 56 days. Similar to the compressive strength test, the splitting tensile strengths of the plain concrete cylinders were found using ASTM C496 procedures. However, since the Group

2 samples were not at the standard moisture content of Saturated Surface Dry (SSD), a slightly modified ASTM C496 procedure was used. The splitting tensile strengths of cylinders are listed in Table 4.

Table 4. Summary of plain concrete cylinder average ulimate tensile strengths.

Sample Age (days)	Ultimate Tensile Strength (ksi)	Group Category
28	0.357	1
49	0.411	1
104	1.36	2
112	1.31	2
119	1.12	2

Due to the different curing times and environments, the stress-strain behavior of Group 1 and Group 2 differ. The differences in the stress-strain behavior between Group 1 and Group 2 are illustrated in Figure 12. The Group 2 samples have significantly higher ultimate splitting tensile stress than the Group 1 samples. Although part of the increase of strength can be attributed to the age of the samples when tested, the differences in the initial slope indicate that the differences in moisture content likely affected the splitting tension strength. The lower moisture content of the samples in Group 2 likely affected the internal friction and cohesion on the macroscopic scale of the concrete and contributed to the Group 2 samples' higher tensile strength. This is consistent with the work of Guo et. al, which suggest that the critical stress needed to fracture the concrete is lowered when the amount of water absorbed is increased (Guo and Waldron, 2001).

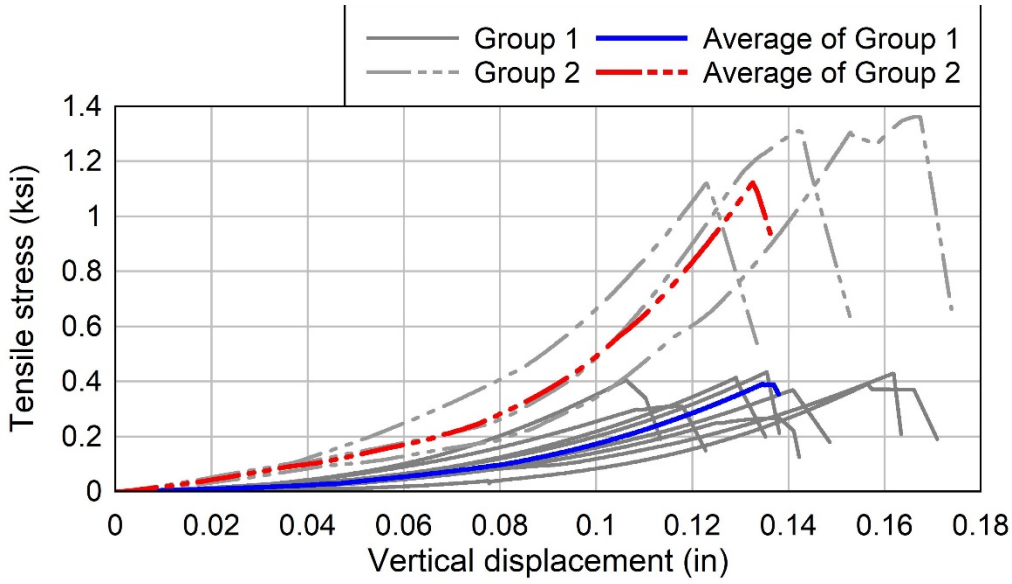

Figure 12. Splitting tension test results of plain 6 inch x 12 inch concrete cylinders.

In addition to the measurements taken by the testing machine (i.e., load and displacement), the tensile behavior was recorded for visual analysis of the crack propagation with a high-speed camera. A Sony RX10 digital camera was used to monitor the fracture mechanisms. The camera is capable of filming 1,000 fps over a four second duration. The typical failure pattern and propagation from an example experiment is shown in Figure 13. Figure (a) denotes the crack initiation and is highlighted for clarity in red. Figure (b) shows the fully formed crack, Figure (c) shows the crack at the ultimate tensile stress, and Figure (d) shows the specimen post-fracture.

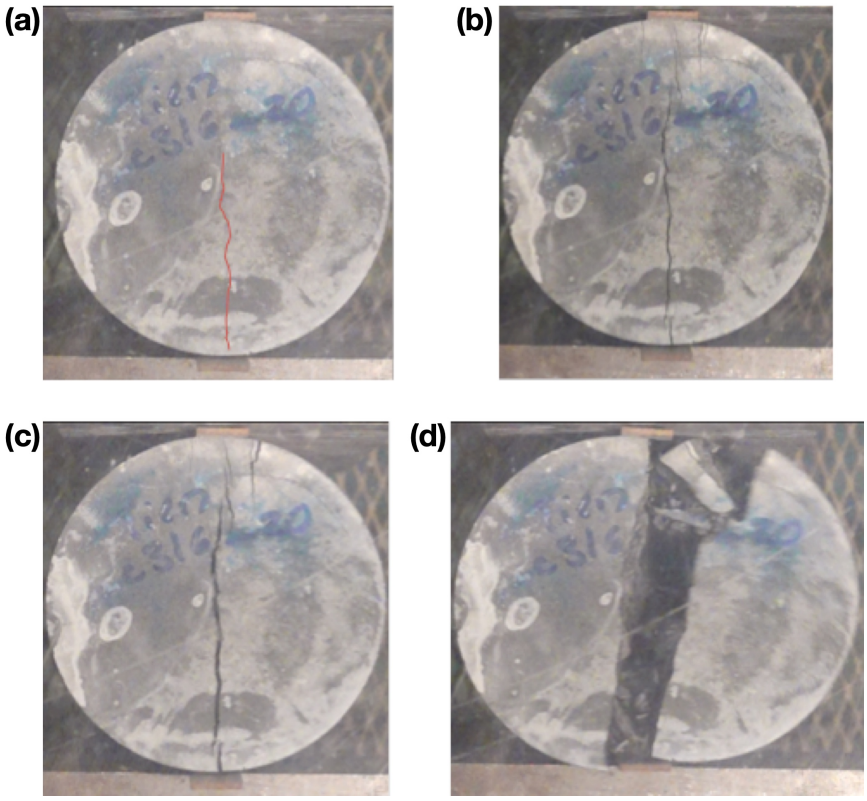

Figure 13. Example tension splitting crack propagation in plain concrete from high-speed camera: (a) crack initiation (highlighted in red for clarity); (b) fully formed crack (c) at failure; (d) post fracture.

Although the split cylinder test can determine the ultimate tensile strength of a specimen, it does not provide an accurate depiction of softening response because of the test's instability and the nonuniform stress gradient (Gergely and Sozen, 1967). As a result, an additional indirect tension test was necessary to determine the required fracture energy needed for the fracture mechanics model. This method is discussed in Chapter 4.

2.2 Epoxy-repaired Concrete Experiments

In addition to the plain concrete cylinders, an experimental procedure was created to evaluate the models' ability to simulate epoxy-repaired concrete cylinders. The epoxy used was a Sealate T-70 High Molecular Weight Methacrylate (HMWM) by Transpo

Industries (see Appendix B). This type of epoxy, recommended by GDOT for this research, is used in situations with thin cracks which require the gravity feed application type. Similar to the plain concrete experiments, the repaired concrete cylinders were tested in uniaxial compression and splitting tension to evaluate the strength and mechanisms of failure.

2.2.1 Specimens

In order to have a controlled cylinder geometry and design, plain concrete cylinders were modified such that they could be repaired with epoxy. Plain concrete cylinders were first cut on a tile cutter lengthwise as illustrated in Figure 14a and b. Then, in order to test the effect of cylinder size, some samples were cut into smaller sections. A series of 6 inch x 6 inch samples and 6 inch x 4 inch samples were created by cutting the lengthwise cut cylinders again as illustrated Figure 14c and d.

Once cut, the two halves' faces were ground flat in order to have a smooth surface for bonding. Construction silicon caulk was then applied to the edges of the sides of the two halves and a slim cardboard spacer was placed at the top and bottom to create a "crack." The two halves were then pushed and tightened together using hose clamps, as illustrated in Figure 15. The silicon caulk was allowed to cure for 24 hours.

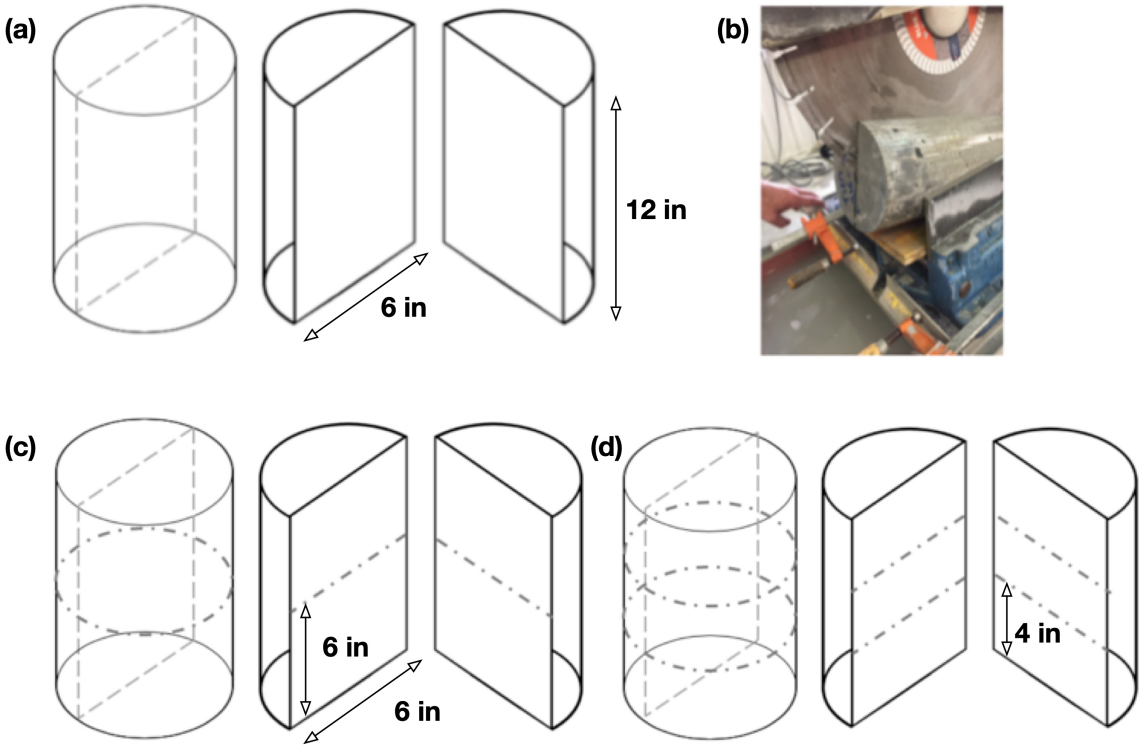

Figure 14. Epoxy-repaired specimens: (a) diagram of lengthwise cut on cylinders; (b) cutting of cylinder on tile cutter; (c) cut locations for 6 inch Samples; (d) cut locations for 4 inch samples.

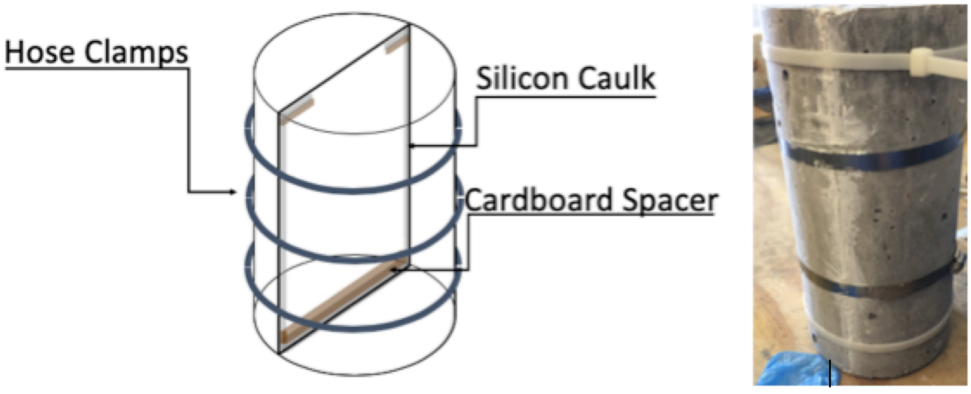

Figure 15. Preparation of epoxy-repaired cylindrical specimen prior to inclusion of epoxy.

The epoxy was a three-part mixture using three ingredients: Cobalt Napthenate promoter, CHP initiator, and propietary Sealate Resin. The ratio of the three ingredients was 75 mL : 150 mL: 1 gal, respectively (Transpo Industries, 2017). The epoxy was created using the following steps:

1. The Cobalt Napthenate was measured in a clean gradient container.
2. The CHP initiator was measured in its own container.
3. The resin was measured in its own container.
4. The resin was poured into a heatproof mixing container, as the reaction is exothermic.
5. The Cobalt Napthenate was added to the resin in the mixing container.
6. The Cobalt Napthenate–resin mixture was stirred for 2 minutes.
7. The CHP initiator was added to the stirred Cobalt Napthenate–resin mixture and stirred again for 2 minutes.

The epoxy was poured into the top opening of the sample until the newly constructed “crack” was completely filled with High Molecular Weight Methacrylate as shown in Figure 16. The epoxy-repaired plain concrete was then allowed to cure for at least 48 hours before testing.

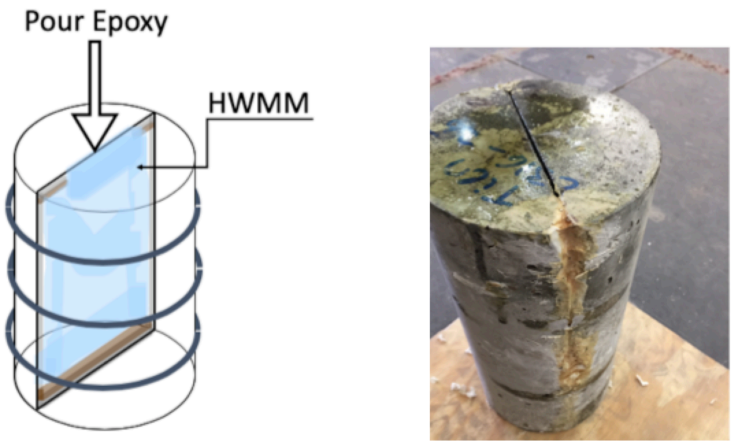

Figure 16. Preparation of epoxy-repaired cylindrical specimen - inclusion of epoxy.

2.2.2 Uniaxial Compression Experiments

Six inch x 12 inch epoxy-repaired concrete cylinders were tested in uniaxial compression. As these pre-repaired concrete cylinders were from the same batch as the plain concrete uniaxial compression cylinders, their sample age at testing was 153 days. Before modifications and repair, the concrete cylinders had cured and aged in the controlled fog room environment for 140 days. After the epoxy repair was completed and the epoxy was allowed to fully cure, the cylinders were tested in uniaxial compression following a procedure based on ASTM C39. This procedure used the same methodology as ASTM C39, but was performed on the repaired concrete cylinders so as to have data that was comparable to the plain concrete uniaxial compression experiments.

The stress-stain behavior of the epoxy-repaired cylinders in compression, compared to the previously described Group 1 and Group 2 compression cylinders is shown in Figure 17. The epoxy-repaired concrete cylinders exhibited a similar elastic modulus as that of the Group 1 plain concrete cylinders. The similarity in modulus is likely due to the fact that the moisture content of the repaired concrete samples was closer to the moisture content of the Group 1 cylinders than the Group 2 cylinders. Using

the interpolation of data shown in Figure 7, it was determined that the approximate compressive strength of the concrete at 153 days is 5.5 ksi. The ultimate compressive strengths of the three repaired specimens are 5.49 ksi, 5.87 ksi, and 6.28 ksi, with an average of 5.88 ksi. It is assumed that the differences of strengths is associated with the the variability of concrete samples in compression, not the epoxy repair.

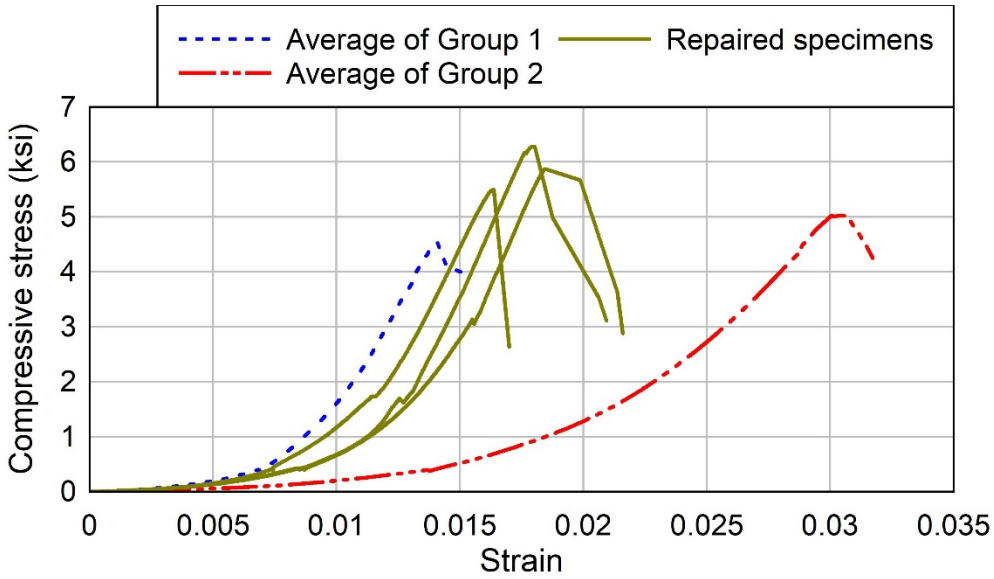

Figure 17. Compressive stress-strain behavior of epoxy-repaired specimens compared with plain concrete cylinder specimens of the same 6 inch x 12 inch size.

During the experiment, the epoxy-repaired cylinders first fractured along the epoxy-repaired spline as shown in Figure 18a and they then failed in a columnar failure mode as shown in Figure 18b. From high-speed camera photographs, it was noted that the repaired concrete cylinders fractured at the concrete/epoxy interface well before any fracture was noticed in the concrete itself. This outcome supports the conclusion that the compressive strength of the repaired concrete is similar to the compressive strength of the plain concrete, as the early fracture of the epoxy-concrete interface does not affect the

load transfer or contribute to any strengthening of the surrounding concrete, which dominates the response.

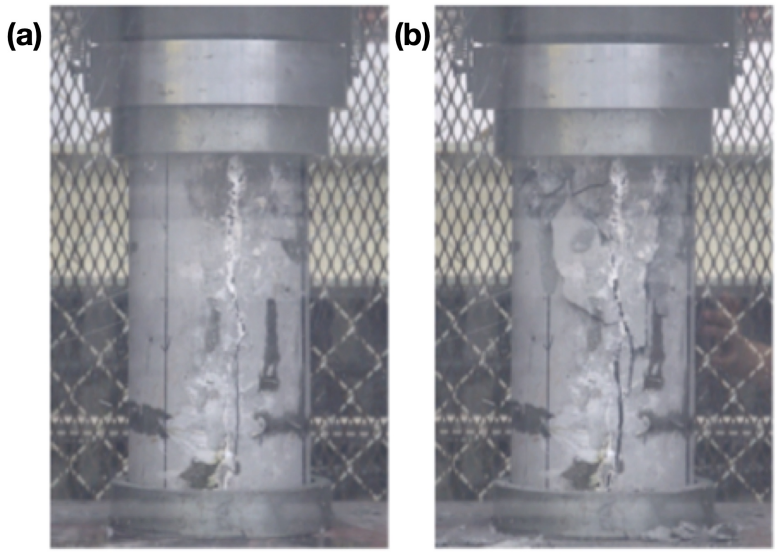

Figure 18. (a) Epoxy-repaired specimen at time 0:19; (b) compressive columnar failure at time 2:59.

2.2.3 Splitting Tension Experiments

Epoxy-repaired concrete cylinders were tested in splitting tension. As these pre-repaired concrete cylinders were from the same batch as the plain concrete splitting tension cylinders, their sample age upon testing was 153 days. Before modifications and repair, the concrete cylinders had cured and aged in the controlled fog room environment for 140 days. After the epoxy repair was completed and the epoxy was allowed to fully cure, the 6 inch x 12 inch splitting tension samples were tested following a procedure based on ASTM C496. This procedure used the same methodology as ASTM C496, but was performed on the repaired concrete cylinders so as to have data comparable to the plain concrete uniaxial compression data. The stress-stain behaviour of the epoxy-

repaired cylinders in splitting tension, compared to the previously described Group 1 and Group 2 samples, is shown in Figure 19.

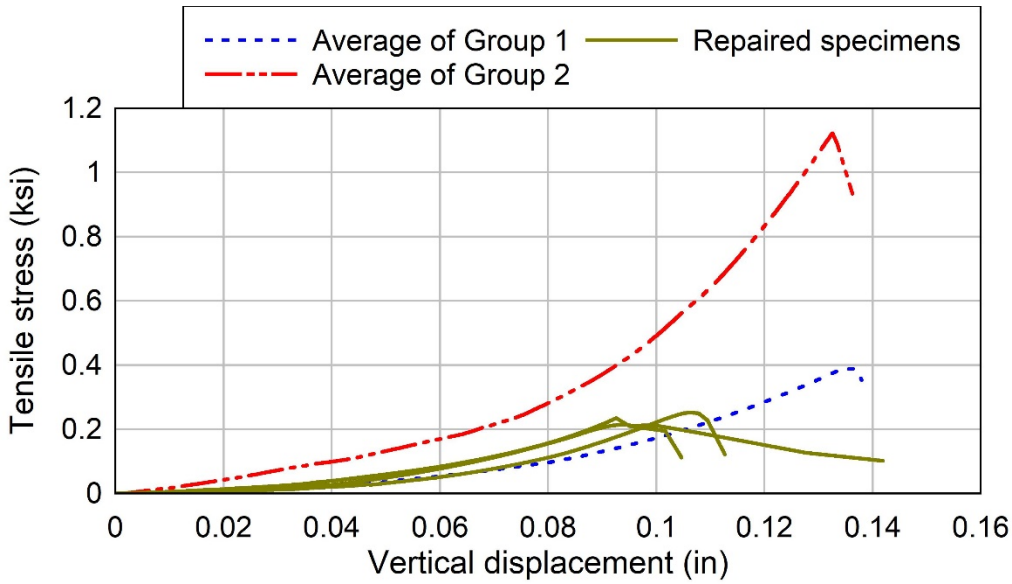

Figure 19. Splitting tension test results of epoxy-repaired cylinder specimens compared with plain cylinder specimens of the same 6 x 12 inch size.

The 6 inch x 12 inch splitting tension epoxy-repaired concrete specimens behaved similarly to the Group 1 plain concrete cylinders in terms of their elastic modulus. Like the repaired concrete compression samples, the repaired concrete tension samples had a moisture content that was more similar to the Group 1 plain concrete samples than to the Group 2 plain concrete samples. However, unlike the repaired concrete compression samples, the repaired concrete tension samples showed a visible decrease in tensile capacity comparised to the Group 1 splitting tension plain concrete cylinders. The decrease in capacity is likely due to the weakness of the epoxy-concrete interface in tension, which involved a smooth surface of the concrete. This theory is supported by the literature, in which is was noted that an increase of surface roughness of concrete subsequently increases the bond adhesion between the epoxy and the concrete due to the

mechanical interlock that a roughened surface provides (Courard, 2014; Czarnecki and Hola, 2016).

As with the plain concrete samples, a high-speed camera was used to capture the crack evolution of the repaired concrete in tension, which allowed for observational details of when and how the epoxy-repaired concrete failed. This is of particular importance for the repaired concrete samples, because the failure initiation location was not clear from post-test visual inspection. It was the high-speed video that demonstrated the interface of the epoxy and concrete was the primary initial fracture location. The typical failure mechanisms of the repaired concrete specimens in splitting tension is shown in Figure 20.

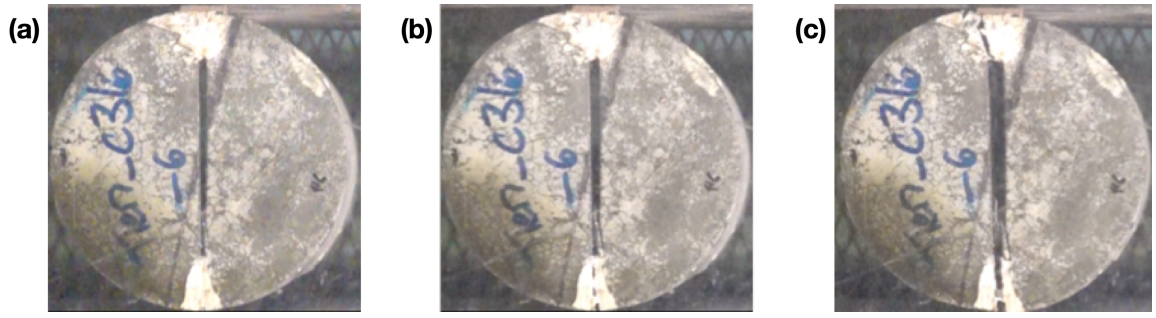

Figure 20. Repaired concrete tension behavior at interface: (a) before failure, (b) crack initiation, and (c) at failure.

2.2.4 Specimen Size Effect for Computational Efficiency

In order to evaluate the effect of sample size of the epoxy-repaired cylinders, six 6 inch x 6 inch and six 6 inch x 4 inch cylinders of epoxy-repaired concrete were tested and compared to the 6 inch x 12 inch cylinders. The primary goal was provide additional data at a reduced size in order to allow using smaller models in Phase II, hence decreasing runtimes. The stress-strain behavior of the repaired cylinder samples in splitting tension is shown in Figure 21 and the results are summarized in Table 5.

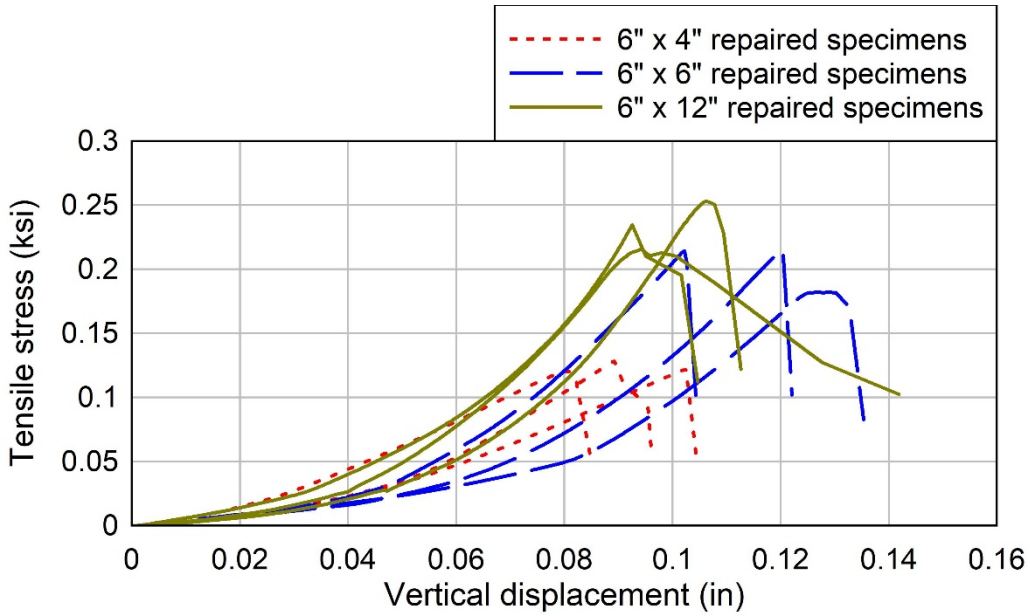

Figure 21. Splitting tension test results of epoxy repaired concrete cylinder specimens of various sizes.

Table 5. Summary of tensile strength of concrete cylinder specimens of various sizes.

Sample Size	Average Tensile Strength (ksi)	Percent Difference From 6 inch x 12 inch
6 inch x 12 inch	0.23	0%
6 inch x 6 inch	0.20	13%
6 inch x 4 inch	0.13	46%

The impact of the dimensions of the repaired cylinder on the average tensile strength was characterized by the percent difference between the average tensile strength of the smaller sample to the average tensile strength of the 6 inch x 12 inch repaired samples. A clear impact of the size of the sample is seen in the testing of the 6 inch x 4 inch samples with a 46% difference with the 6 inch x 12 inch samples. In comparison, the difference between the 6 inch x 6 inch samples and the 6 inch x 12 inch samples was only 13%. As such, it was recommended that the smallest size the model should use was a 6 inch x 6 inch cylinder in order to minimize the size effect on the ultimate tensile strength of epoxy-repaired concrete.

CHAPTER 3. MORTAR CYLINDER EXPERIMENTS

3.1 Plain Mortar Experiments

DEM models in Phase II are tasked with characterizing fracture patterns in plain concrete. The models require calibrating the mechanical parameters of particulate elements and bonds. The calibration is done in two steps: (i) calibration of the parameters of particulate elements and bonds in mortar; (ii) calibration of the parameters of particulate elements and bonds in aggregates and calibration of the parameters of the mortar/aggregate bonds. In order to fulfill objective (i), mortar cylinder tests were conducted. Similar to plain concrete, a series of tests were developed to evaluate the fracture behavior in the mortar subjected to both uniaxial compression and splitting tension loads. The Phase II models were then validated by simulating the location and behavior of microcracks in the mortar matrix, coarse aggregate, and at the interface of the two throughout the duration of a tensile splitting experiment simulation.

3.1.1 Material

The mix design of the mortar was very similar to the mix design used in the plain concrete cylinder experiments. The mortar samples were made using the same ratio of cement to water (0.38) and the same ratio of cement to fine aggregates (0.72) as for the mortar matrix of the plain concrete samples. The mix design of mortar used is given in Table 6.

Table 6. Mortar mix properties.

Material	Weight Fraction
Cement	36%
Water	50%
Fine Aggregates	14%

The mortar was mixed by hand using the following steps:

1. The fine aggregate (sand) and cement were added to a large container
2. The sand and cement were fully mixed together using a mortar hoe
3. The water was added to mixture
4. The mortar mixture was fully combined using a mortar hoe
5. The mixture was poured into cylinder molds

3.1.2 Specimens

Two batches of mortar were produced. The first batch of mortar was made to determine the size effect of the mortar cylinders for specimen selection. Due to computational constraints, the model could only consider cylinders of 6 inch x 6 inch in tension. Sample sizes of 6 inch x 4 inch, 6 inch x 3 inch, and 6 inch x 2 inch are more computationally efficient. In order to ensure the most reliable tests, experiments were conducted to find the sample size that ensured the most consistent results. The following samples were cast and tested:

- Three 6 inch x 12 inch mortar in splitting tension
- Three 6 inch x 4 inch mortar in splitting tension
- Three 6 inch x 3 inch mortar in splitting tension
- Two 6 inch x 2 inch in splitting tension

The tensile stress-strain results of the splitting tension experiments for specimens of various sizes are shown in Figure 22. A summary of the average ultimate values as well as the coefficients of varitaion (COV) are given in Table 7.

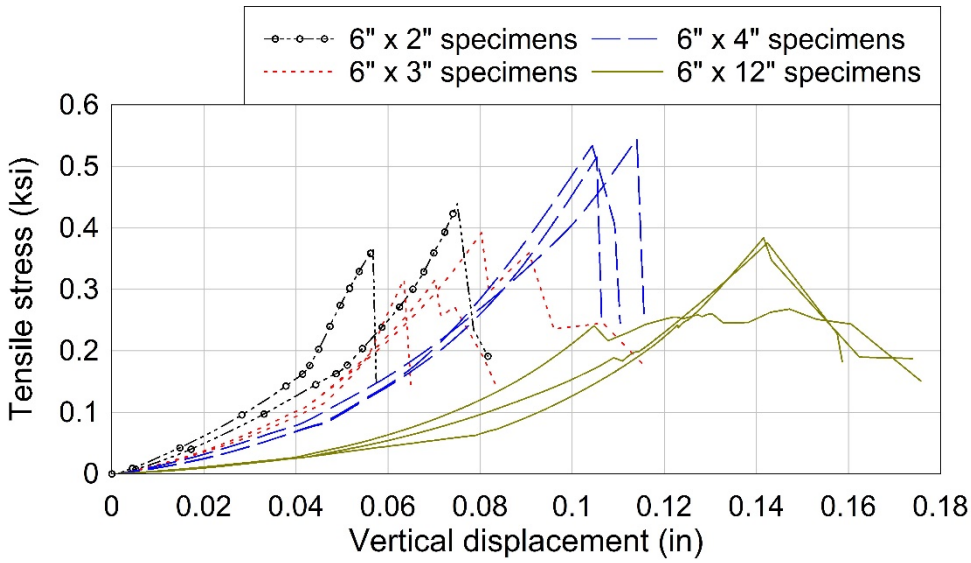

Figure 22. Splitting tension test results of mortar cylinder specimens of various sizes.

Table 7. Summary of average tensile strength and coeffiecient of variation of mortar specimens of various sizes.

Sample Size	Average Tensile Strength (ksi)	Coefficient of Variation (COV)
6 inch x 12 inch	0.351	18%
6 inch x 4 inch	0.558	3%
6 inch x 3 inch	0.376	12%
6 inch x 2 inch	0.455	N/A

The choice of which specimen size to use was judged based on the cofficient of variation (COV) of each size, consistency in failure mode, and average tensile strength. According to the literature, mortar alone should have a higher strength than the equivalent concrete matrix with the same water to cement ratio (Hillerborg, 1985; Alexander and Mindess, 2014). The 6 inch x 4 inch samples were chosen because they

had the lowest COV, provided the most consistent failure mode, and had a tensile strength greater than the concrete at 28 days. An example of the 6 inch x 4 inch typical breaking pattern is illustrated in Figure 23.

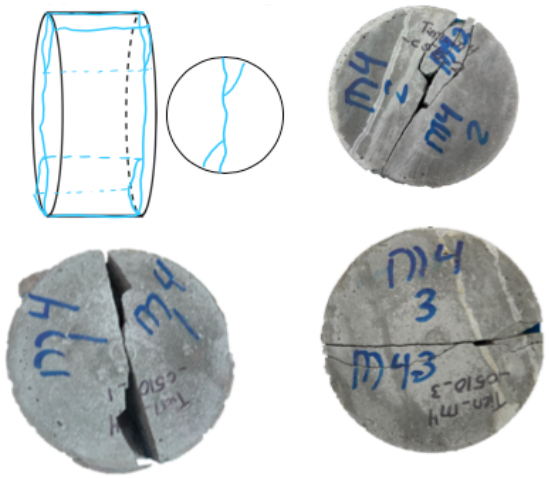

Figure 23. Typical failure patterns of a 6 inch x 4 inch mortar specimen.

3.1.3 Compression Experiments

A second batch of mortar using the same mix design and process was produced. This mixture was used to cast 6 inch x 4 inch mortar tension samples and 4 inch x 8 inch mortar compression samples. The results of the compression experiments are presented in this section and the following.

The 4 inch x 8 inch mortar compression specimens were tested to find the uniaxial compression strength using a method based on ASTM C39. The compressive stress-strain behaviour for the three samples is shown in Figure 24. The average compressive strength of the mortar was 9.53 ksi. Consistent with the literature, the compressive strength of the mortar was found to be roughly twice that of the plain concrete with the same water content. The shear and columnar failure patterns exhibited by the mortar samples in compression are shown in Figure 25.

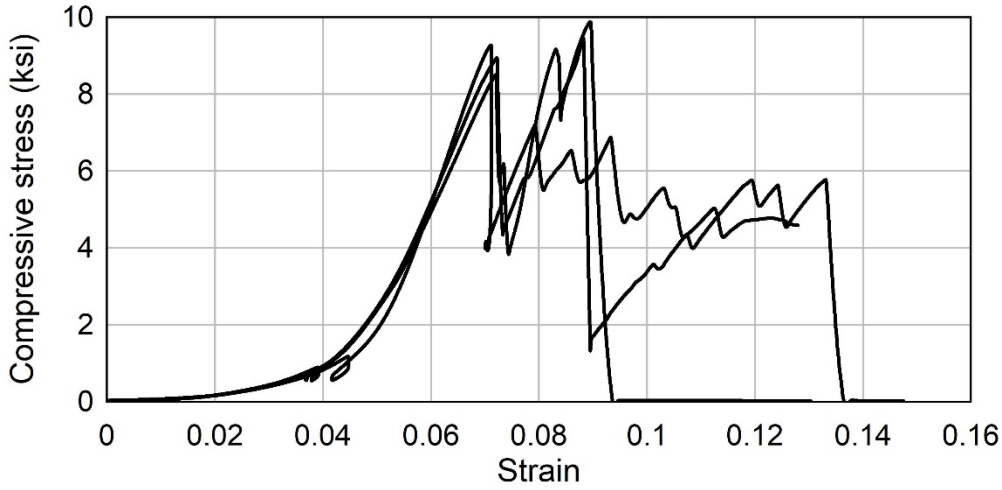

Figure 24. Compressive test results of mortar 4 inch x 8 inch cylinder specimens.

Figure 25. Typical failure pattern of a mortar specimen.

3.1.4 Splitting Tension Experiments

The 6 inch x 4 inch mortar tension specimens made of the second batch were tested to determine the splitting tensile strength using a method based on ASTM C496. In addition to the 6 inch x 4 inch samples, the three 4 inch x 8 inch mortar samples were tested to obtain additional comparative data points for future research as the computer models are refined. The splitting tensile stress-strain curves are shown in Figure 26.

Consistent with the literature (Monteiro, 2006; Alexander and Mindess, 2014), the splitting tensile strength of the mortar (0.68 ksi) was found to be roughly twice that of the plain concrete (0.36 ksi) at the same water content. An example of the typical crack propagation of the 6 inch x 4 inch mortar sample is shown in Figure 27. The figure shows the specimen before any cracks develop, at the onset of cracking near the midline, and the specimen at the ultimate tensile strength.

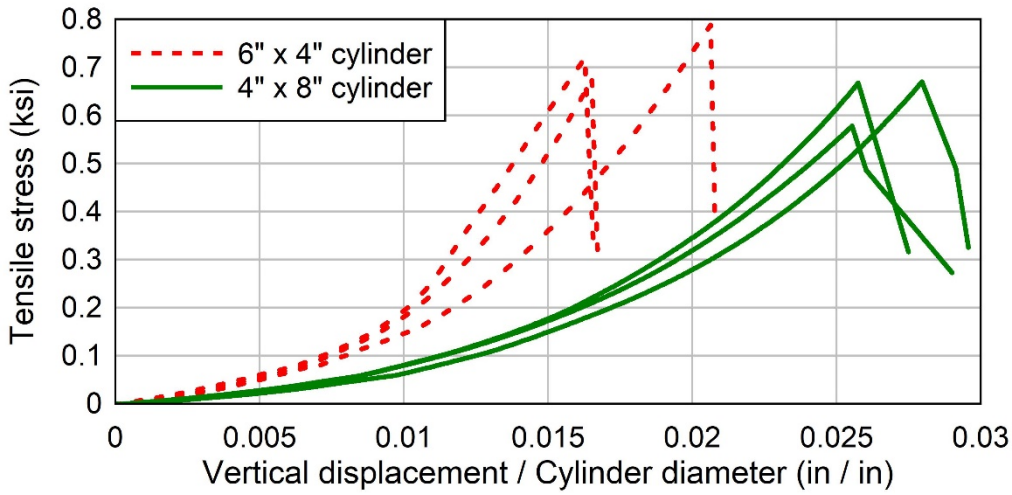

Figure 26. Splitting tension test results of mortar cylinder specimens of various sizes.

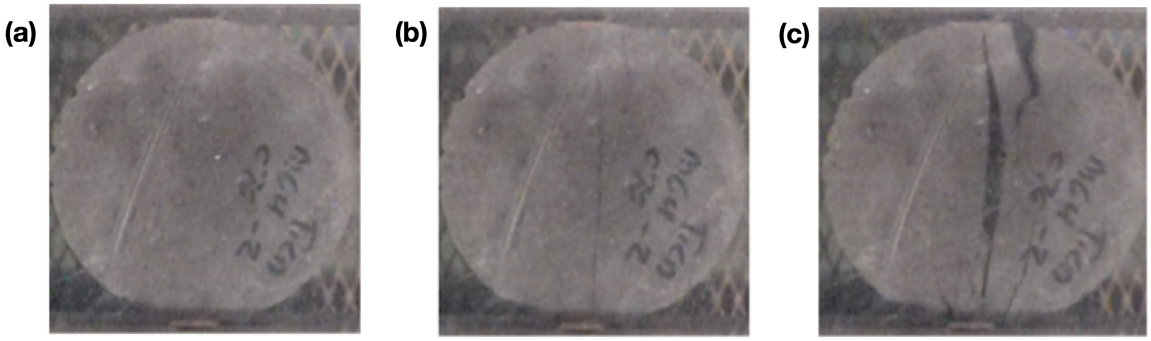

Figure 27. Behavior of mortar during splitting tension test: (a) before crack develops; (b) at onset of cracking; (c) at ultimate strength.

CHAPTER 4. BEAM EXPERIMENTS

The experiments presented in this chapter are divided into two categories: unreinforced concrete beam experiments (Section 4.1) and reinforced concrete beam experiments (Section 4.2). For both categories, experiments were conducted on "as-built" and epoxy-repaired concrete beams.

4.1 Unreinforced Beam Experiments

The unreinforced beams were designed to be experimentally characterized using Hillerborg's three-point bend test. To determine the flexural strength and fracture energy of the concrete, a specialized three-point bend test on a notched beam was used. This test was derived from Hillerborg and others' experiments during their development of the ficitious crack model (FCM) (Hillerborg, 1985). A diagram of the fracture energy three-point bend test developed by Hillerborg is shown in Figure 28. With some geometric design variations, multiple past studies successfully used this method to find the fracture energy of concrete (Bazant, 1992; Lee and Lopez, 2014).

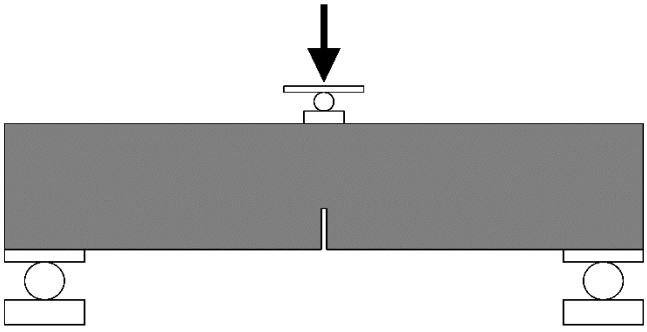

Figure 28. Schematic of notched three-point bend test.

4.1.1 Specimens

The unreinforced beams were cast using the same concrete that was used to produce the concrete cylinders discussed in Section 2.1.2. Since the three-point bend test is sensitive to the length of the beam, beams of both three-foot and four-foot lengths were cast using in-house using wooden formworks, shown in Figure 29. Beams of both lengths had a cross-section of 6 inch x 10 inch. Drawings of the beams are included in Appendix A. Seventy-two hours after casting, the beams were demolded and placed in a controlled fog room environment for curing. At 56 days, the beams were removed from the controlled environment and allowed to age at ambient temperatures until their test date. As previously discussed in Chapter 2, plain concrete cylinder samples were tested in uniaxial compression and splitting tension each week throughout the duration of beam testing to quantify the compressive and tensile strength of the beam. The unreinforced beams were notched using a masonry saw to a notch depth of 3.25 inch, shown in Figure 30.

Figure 29. Concrete beam formwork.

Figure 30. Notching of concrete beams with masonry saw.

To achieve a "repaired" concrete state, the unreinforced beams of both 3 feet and 4 feet of length were cut completely into two halves and then reattached by the same HMWM epoxy as the one used in the repaired concrete cylinders. The following describes the methodology used to prepare the unreinforced beam for repair with epoxy:

1. The unreinforced beam was cut into two halves with a masonry saw (Figure 31).

Figure 31. Preparation of epoxy-repaired beam: beam cut in half with masonry saw.

2. The notched region was prepared by inserting a single wall corrugated cardboard with thickness of 0.125 inch between the two halves (Figure 32a).
3. Construction silicon caulk was applied at the border of the repaired section on one half of the beam (Figure 32b).

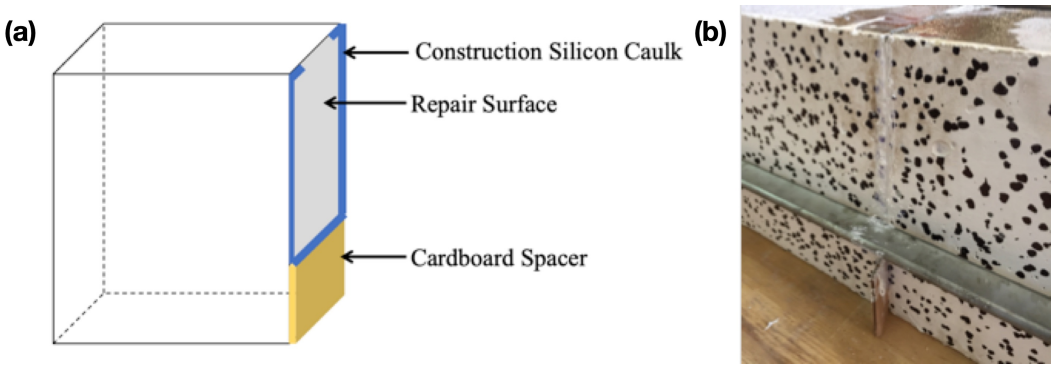

Figure 32. Preparation of epoxy-repaired beam: (a) diagram of silicon caulk and spacer placement; (b) silicon edging and cardboard spacer.

4. The two halves were compressed together, making sure they were aligned, and were tighten using long clamps (Figure 33).

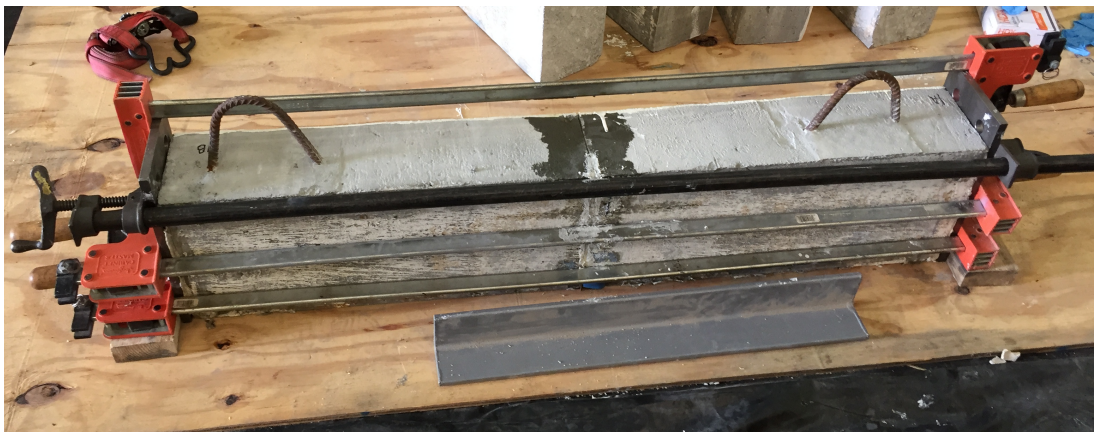

Figure 33. Preparation of epoxy-repaired beam: repaired beam clamped together for curing.

5. Any silicon that escaped the notch was smoothed out and more silicon was applied to securely seal the repaired section, if needed.
6. The silicon was allowed to cure for at least 24 hours before applying epoxy.

Once the silicon was cured, the HWMM was mixed. The epoxy was a three-part mixture using three ingredients with a 75 mL:150 mL:1 gal ratio of Cobalt Napthenate promoter, CHP initiator, and propietary Sealate Resin, respectively (Transpo Industries, 2017). The epoxy was mixed with the same steps as with the epoxy-repaired cylinders, given in Section 2.2.1. The epoxy was then poured into the created "crack," shown in Figure 34a. Steel plates were used to guide the epoxy into the "crack" until it was completely full of the HWMM as shown in Figure 34b. After the crack was filled with epoxy, sponge paintbrushes were used to ensure the crack was completely filled with epoxy and level with the top of the beam. The epoxy was allowed to set for at least 48 hours.

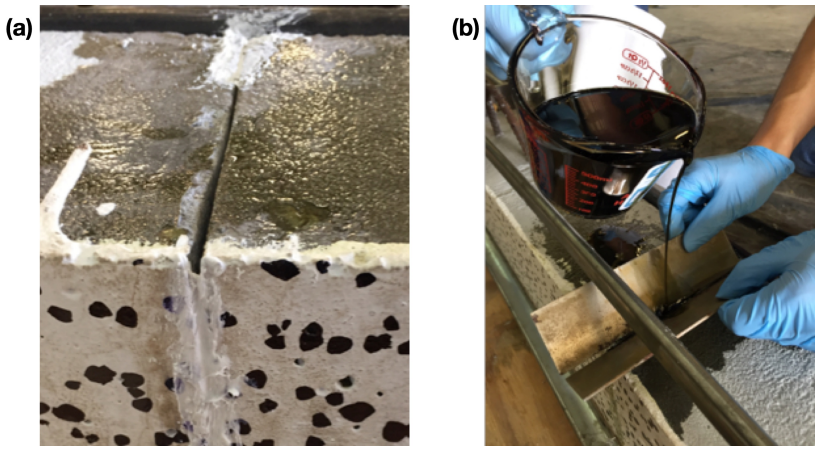

Figure 34. Preparation of epoxy-repaired beam: (a) "crack" opening of the repaired concrete beam; (b) pouring epoxy into "crack"

4.1.2 Experimental Setup

The setup of the three-point bend experiment is shown in Figure 35. A 50-kip, Interface 1220AO-50k load cell was connected to an Interpac hydraulic jack to apply a load at a rate of approximately 2 kips per minute. The notched unreinforced beams were set on roller supports to limit the effect of friction on the results. As the focus of these tests was to determine the fracture energy of the concrete, the two measurements of interest were global deflection and crack opening versus the load applied.

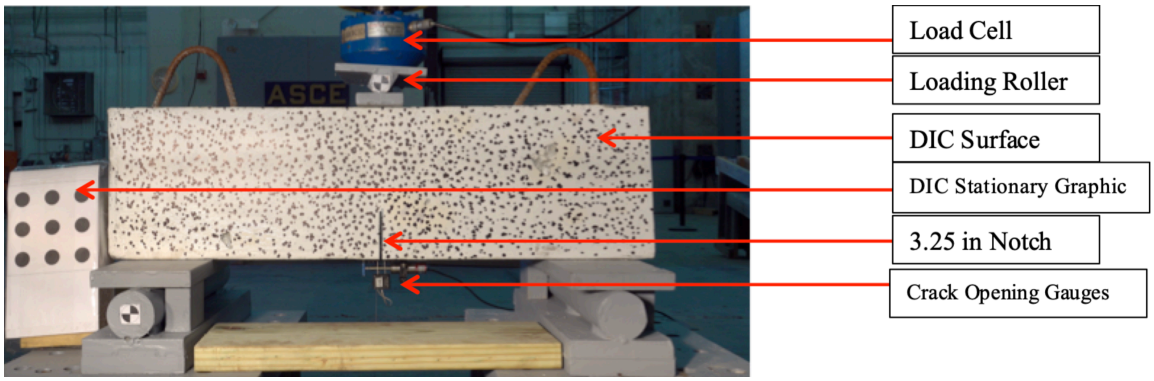

Figure 35. Three-point bend experimental setup.

To ensure redundancy in measuring the crack opening, two methods of measurement were used: a lateral variable differential transmitter (LVDT) and an extensometer. The RDP DCTH200AG LVDT used in this experiment had a maximum travel of +/- 0.2 inch. The extensometer used in this experiment was an MTS 6.3203E-20 clip-on extensometer with a maximum travel of +/-0.15 inch. Both measuring devices are shown in the photo in Figure 36.

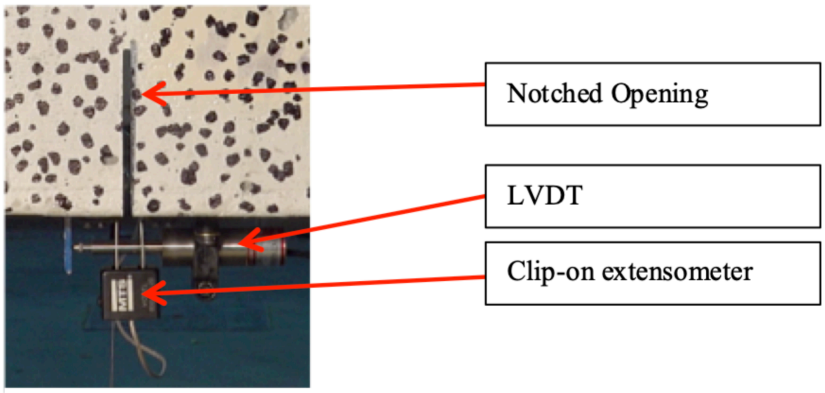

Figure 36. Crack opening instrumentation: LDVT and extensometer.

To ensure redundancy in measuring the global deflection of the beam, two methods of measurement were used: a stringpot gauge and digital image correlation (DIC). A Celesco PT1A-50-UP-500-M6_SG stringpot gauge was connected to a hook attached to the front face of the beam. This attachment is shown in Figure 37. The hook was connected to the beam using a small L-brace and fishing wire in order to prevent warping in the string pot.

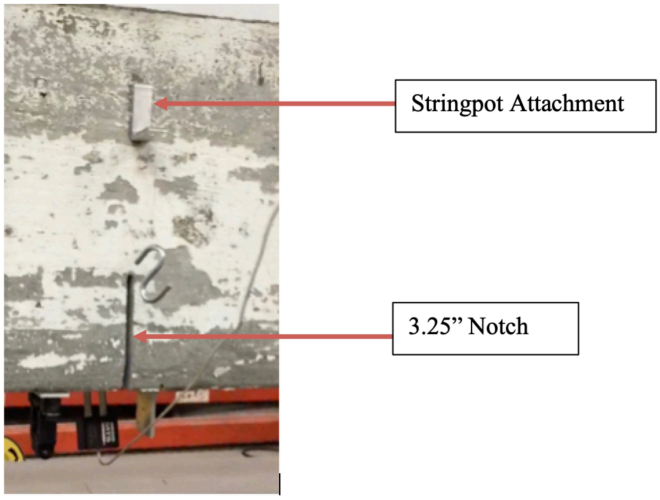

Figure 37. Deflection instrumentation: stringpot.

Digital Image Capture (DIC) was used to globally evaluate how the beam reacted to the applied load. A Sony RX10 Digital camera, which is capable of filming 1,000 fps

over a four second duration was used to measure the beam, which had its entire front face painted white and marked with black dots for tracking. This treatment is referred to as a "DIC surface," for simplicity. Although, the DIC system was not sensitive enough to measure the relatively small deflection of the unreinforced notched beams before total failure, it did provide valuable information about the beam's global behavior. As a result, the stringpot was the main source of quantitative deflection data for the unreinforced notched beams.

4.1.3 Results

One of objectives of the three-point bend test was to find the fracture energy directly from the unreinforced notched beams. The crack mouth opening displacement was successfully captured by both the extensometer and the LVDT until the peak load. After peak load, the beams failed in a brittle maner within a short period of time, usually less than 1 second. As a result of this brittle failure and the associated sudden dramatic increase of crack opening, the extensometer and LVDT typically detach from the beam. Therefore, the results were reliably captured until the peak load but not after the peak load.

4.1.3.1 Three-foot Beam Experiments

Five three-foot beams were successfully tested: three "as-built" specimens and two epoxy-repaired specimens. The applied load versus deflection behavior and the corrosponding crack opening displacement of the three-foot unreinforced notched beams are shown in Figure 38. In general, the epoxy-repaired beams performed better in terms of ultimate capacity than the intact concrete beams and also exhibited a slightly greater stiffness. An image of the typical failure of an "as-built" unreinforced notched three-foot

beam can be seen in Figure 39 and the epoxy-repaired behavior can be seen in Figure 40. The epoxy-repaired concrete exhibited cracking within the concrete rather than along the interface.

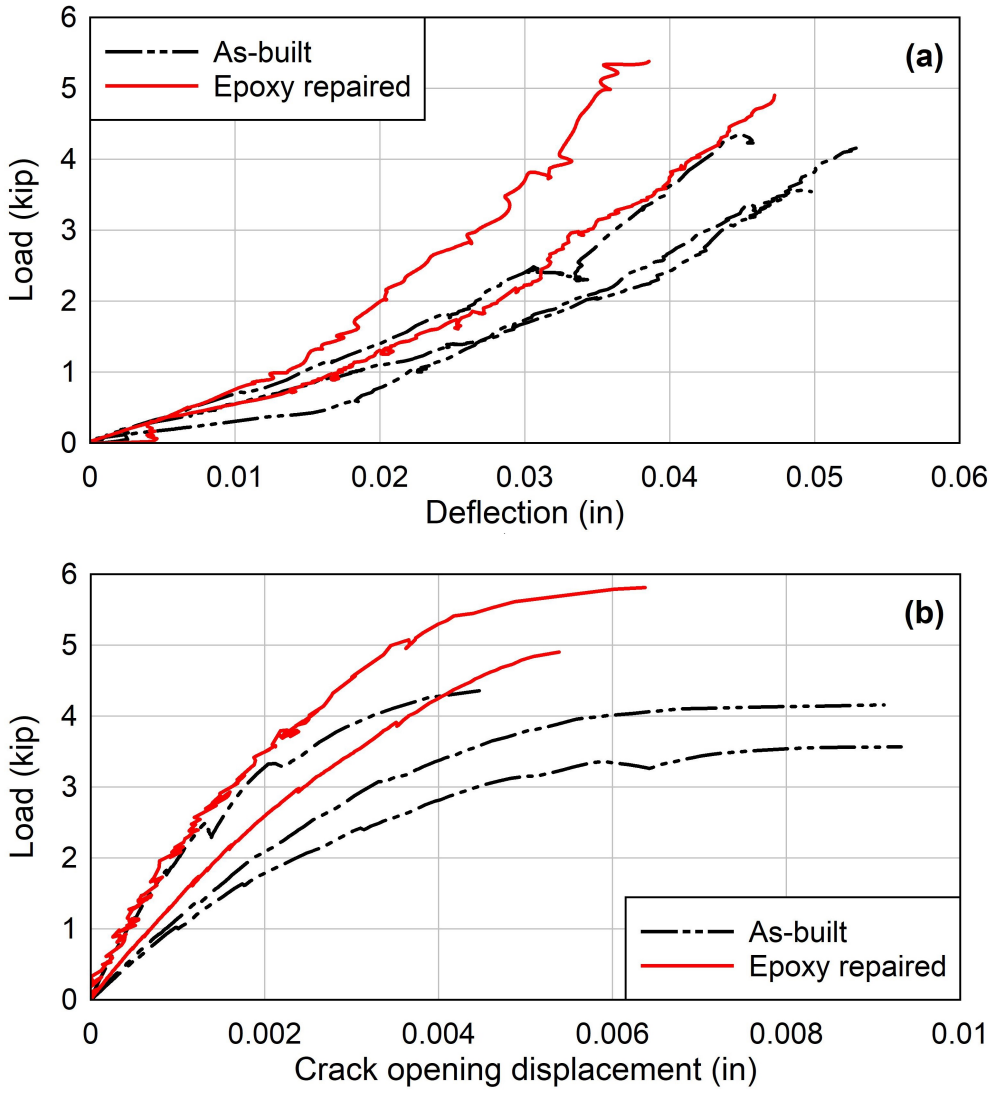

Figure 38. Test results of three-foot unreinforced concrete beams: (a) applied load versus vertical deflection at mid-span; (b) applied load versus crack opening displacement at mid-span.

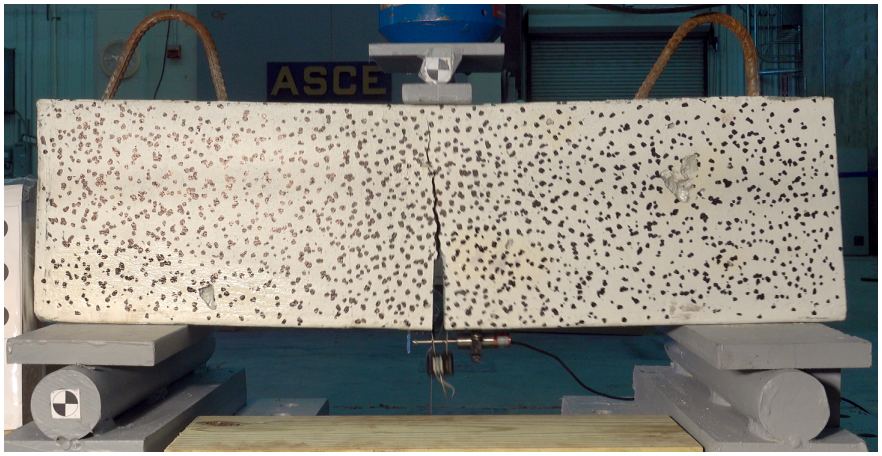

Figure 39. Three-foot "as-built" unreinforced concrete beam behavior.

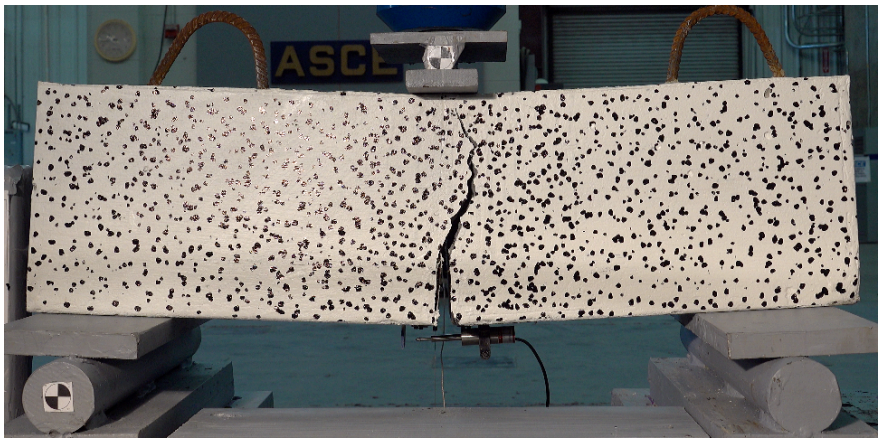

Figure 40. Three-foot epoxy-repaired unreinforced concrete beam behavior.

4.1.3.2 Four-foot Beam Experiments

After testing the three-foot beams, four four-foot beams were tested: two "as-built" specimens and two epoxy-repaired specimens. The experimental setup was altered to accommodate the larger beams by moving the location of the roller supports on the reaction frame. The load versus deflection curves and the corrosponding crack opening displacement of the four-foot unreinforced notched beams is shown in Figure 41. Similar to the three-foot beams, the epoxy-repaired beams, in general, performed better in terms of ultimate capacity than the "as-built" concrete beams. A photo of the typical failure of

an “as-built” unreinforced notched four-foot beam can be seen in Figure 42 and the epoxy-repaired behavior can be seen in Figure 43. The epoxy-repaired concrete exhibited cracking within the concrete rather than along the interface.

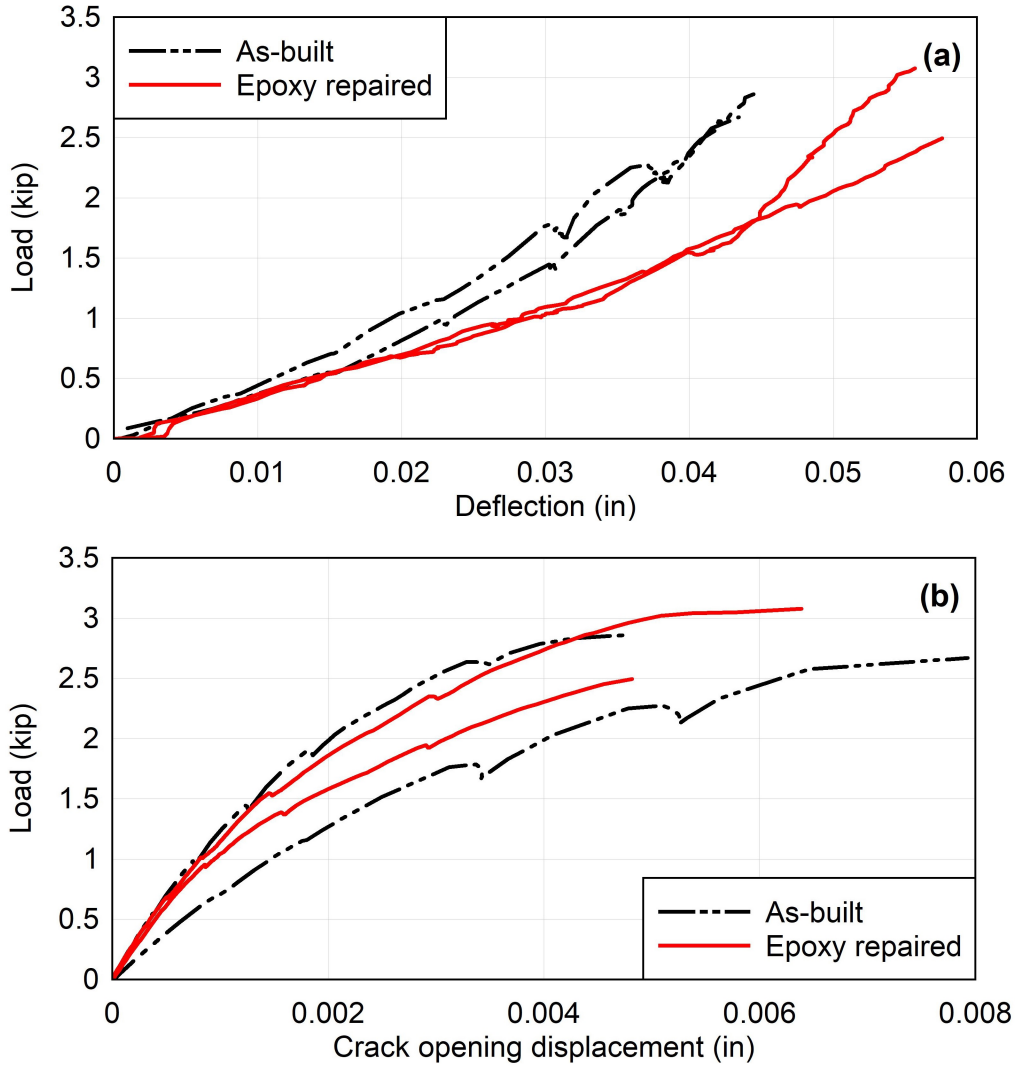

Figure 41. Test results of four-foot unreinforced concrete beams: (a) applied load versus vertical deflection at mid-span; (b) applied load versus crack opening displacement at mid-span.

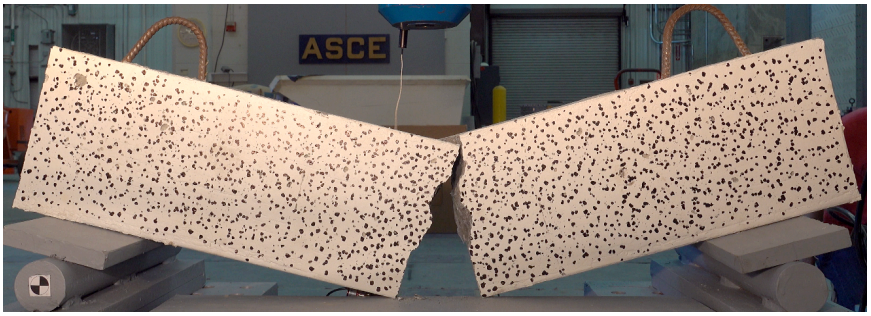

Figure 42. Four-foot "as-built" unreinforced concrete beam behavior.

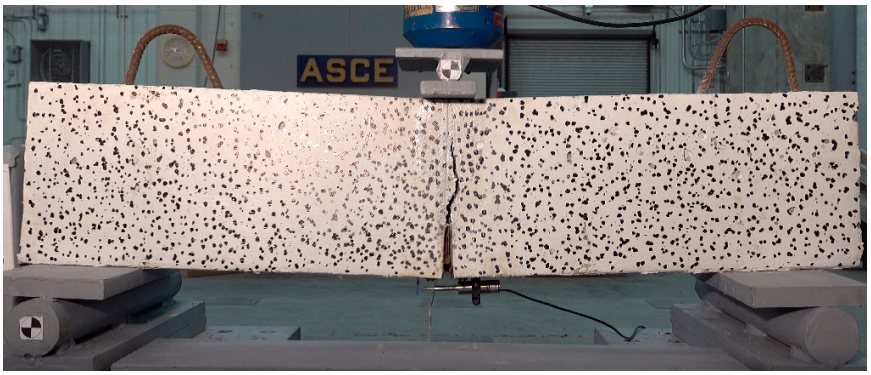

Figure 43. Four-foot epoxy-repaired unreinforced concrete beam behavior.

4.2 Reinforced Beam Experiments

The second beam type tested were reinforced concrete beams and included experiments of both "as-built" and epoxy-repaired specimens. In total, four reinforced concrete beams were tested. These beams were used to understand and quantify the effect of epoxy repair of various size cracks on the beam's capacity with an application that is similar to that in the field.

4.2.1 Specimens

The beams were constructed in a manner similar to those described in Section 4.1.1, but these beams had the inclusion of reinforcing steel and no notch was cut. The beams were cast on the same day as the notched beams and the concrete cylinders. Thus, the cylinder experiments of Chapter 3 can be used to quantify the material parameters of the beams. The beams were 4 feet in length and had a 6 inch x 10 inch cross section. The beams were longitudinally reinforced with two #6 rebars of 60 ksi steel. Structural drawings are located in Appendix A.

4.2.2 Experimental Setup & Procedure

The reinforced concrete beams used the same test setup as the unreinforced beams, except that crack monitoring gauges were not used because there was no notch. Instead, only the stringpot and DIC were used to measure the beam's deflection. The first experiment used a beam in its "as-built" configuration. The beam was tested to failure. The failure of the control beam is shown in Figure 44. This beam was used to observe the various crack sizes that were formed under different applied loadings (with associated displacements).

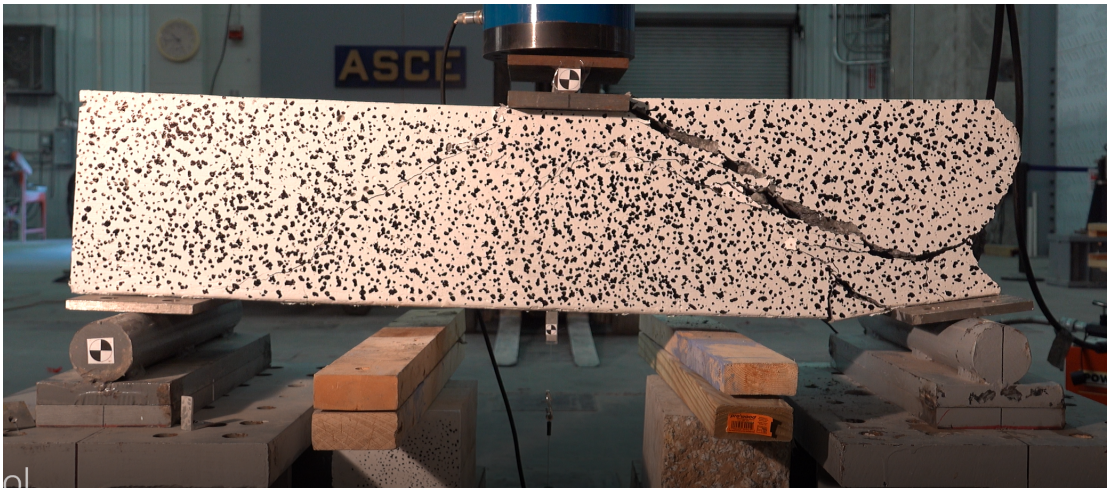

Figure 44. Behavior of "as-built" reinforced concrete beam at failure.

The remaining three reinforced concrete beams were loaded until minor hairline cracks (second beam) and major cracks (third and fourth beam) formed. Note that the definition of "minor" and "major" cracks was internal to Georgia Tech and does not necessarily correspond to any internal GDOT definitions of crack sizes. "Minor cracking" refers to cracks under the 0.006 in PCI minimum for epoxy injection. "Major cracking" refers to cracks at or above that limit. Once the cracks developed, the beams were unloaded and prepared for repair using the epoxy. The beams were removed from the frame and laid on their sides. The change in orientation of the beam allowed gravity to assist the epoxy flow as it filled the cracks. The epoxy and its preparation were the same as the previous concrete repair experiments. The epoxy was applied by coating the surface of the beams with several layers of epoxy using a foam paintbrush. Once applied, the epoxy was allowed to cure for at least 48 hours before testing. Once fully cured, the beams were placed back on the testing frame and tested to failure using the same three-

point bend test setup as was used in the four-foot unreinforced four-foot beam experiments.

4.2.3 Results

The load versus deflection curve of the "minor crack" repair beam in comparison to the "as-built" beam is shown in Figure 45. The first peak shown on the graph represents the loading until the minor crack formed, as shown in Figure 46a. At this point, the beam was unloaded and repaired by epoxy. After the epoxy repair had finished curing, the beam was reloaded until the second peak occurred. Marked on the graph, this point represents the failure of the beam post-repair. This failure can be seen in Figure 46b. The repaired reinforced beam with minor cracking had a capacity similar to the "as-built" beam. In addition, the failure pattern of the repaired beam and the "as-built" beam were very similar. However, the "minor crack" repaired beams exhibited a more brittle behavior than the "as-built" beam, notably having a large reduction in capactity at about 25% of the ultimate strain of the "as-built" beam.

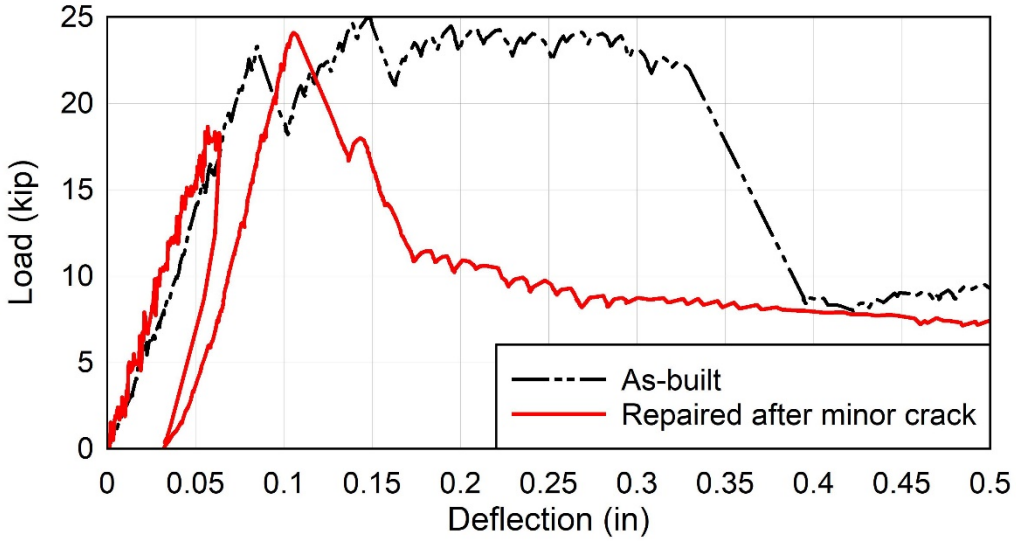

Figure 45. Load-deflection behavior of reinforced concrete beam repaired after minor cracks compared to as-built beam.

Figure 46. Behavior of reinforced concrete beam: (a) at minor crack development; (b) at failure.

The experiment was repeated on two beams that exhibited major cracks before repair. The load versus deflection behavior of the "major crack" repaired beams in

comparison to the "as-built" beam is shown in Figure 47. The first peak shown on the graph represents the loading until the major crack formed. The DIC analysis of this is shown in Figure 48a. As shown in the analysis, the major crack appears in the concentrated red section as the dots in this region displaced the most from their original position. The second peak before complete failure represents the capacity of the beam after the epoxy repair. The DIC analysis of this event is shown in Figure 48b and a posttest photo is shown in Figure 49. In both cases, the beams repaired by epoxy after a major crack had developed were able to sustain approximately twice the load of the "as-built" beam. Interestingly, the failure strains of the beams were not the same and in one case, the failure strain was significantly less than the failure strain of the "as-built" beam.

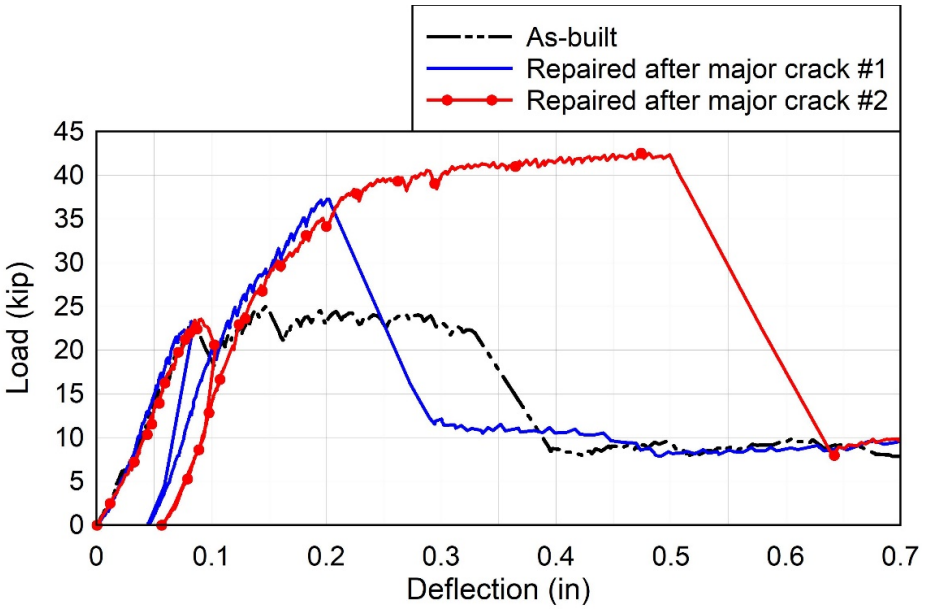

Figure 47. Load-deflection behavior of reinforced concrete beams repaired after major cracks compared to as-built beam.

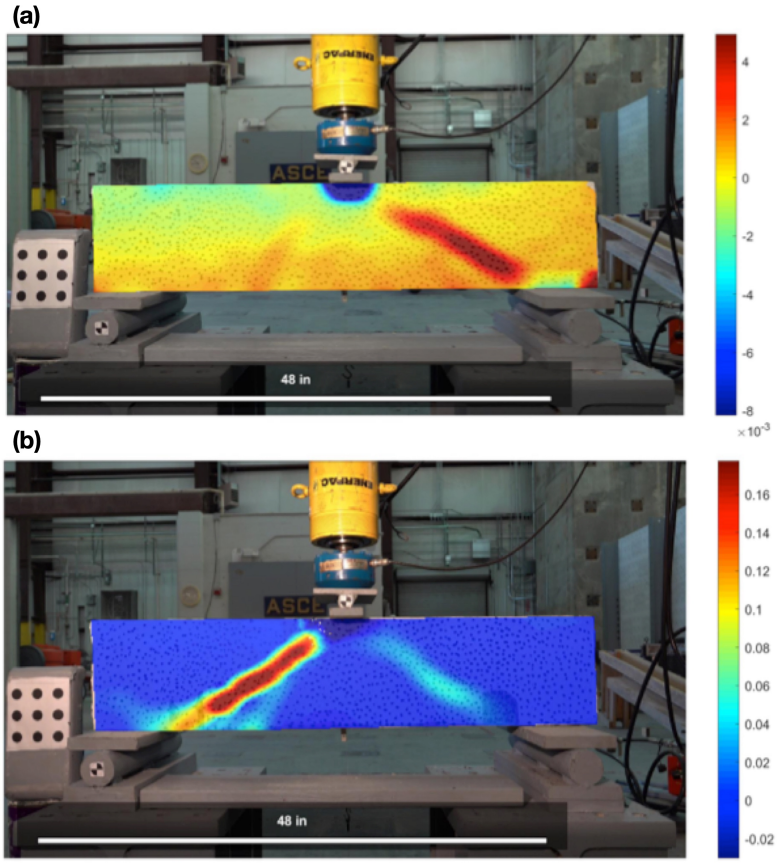

Figure 48. Behavior of epoxy-repaired reinforced concrete beam via DIC: (a) at major crack development; (b) at failure. Values in inches.

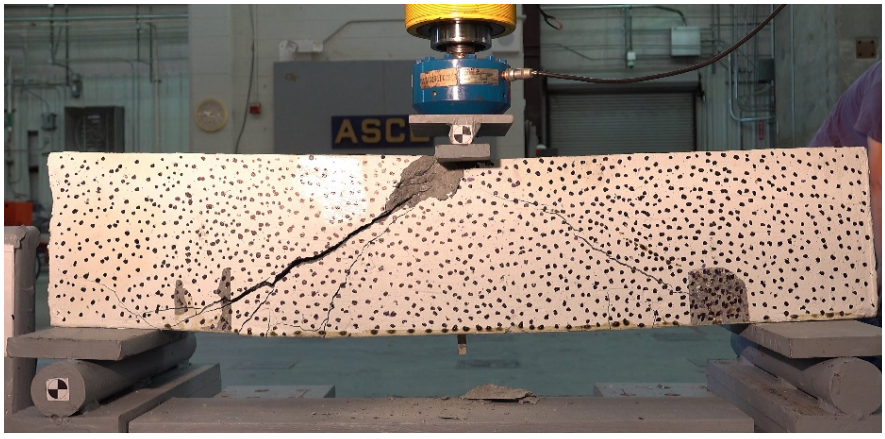

Figure 49. Behavior of epoxy-repaired reinforced concrete beam at failure.

The beams that were repaired after major cracks showed significant increases in capacity compared to both the as-built beam and the beam repaired after minor cracking.

One possible reason is that the relatively wider cracks on the beams loaded to major cracking allowed the epoxy to penetrate more deeply into the beam. During the repair of beams after major cracking, visible epoxy droplets formed on the other side of the beams, indicating that the epoxy went through the entire section of the cracked beams. In contrast, this phenomena was not observed during the repair of the beam after minor cracking, indicating that the relatively narrower cracks on the beam loaded to minor cracking tended to prevent the epoxy from fully penetrating.

Another possible reason for this capacity change is that epoxy repair may alter the force distribution inside the beam, and thus, the failure mechanisms and changed the overall capacity. As Figure 48 shows, major cracks appeared on the right side of the beam when initially loaded. After unloading and repairing, the beam failed with major cracks on the left side when it was loaded again. This is possibly because the epoxy repair penetrated into the right side of the beam through major crackes, which occurred during initial loading. This increased the strength of the local region on the right hand side. As a result, when the beam was loaded again, the left side was relatively weaker than the right side. Because of this difference in strength, the beam started to form new cracks at the left side instead of reopening the existing repaired cracks on the right side. The increase of ulitimate capacity may be related to the formation of new cracks on the left side of the beam.

CHAPTER 5. SUMMARY & CONCLUSIONS

The main contributions and conclusions from the the Phase III research project as are follows:

1. The research team developed and executed an experimental method to characterize epoxy-repaired concrete cylinders via uniaxial compression and splitting tension. The experiments, which included cutting plain concrete cylinders and repairing them using epoxy, were conducted to provide mechanical properties as well as qualititative data (via high-speed cameras) to calibrate the Phase II models.
2. Uniaxial and splitting tension experiments were conducted on plain mortar cylindrical specimens in order to provide mechanical properties of the mortar as a separate material. Studies on specimen size effect were conducted in order to determine the most computationally-efficient DEM sample size for the Phase II models.
3. Unreinforced concrete beam experiments were conducted on notched specimens. These tests included both plain concrete beams and beams that were repaired with an epoxy layer at a cut made directly above the notch. In all experiments involving the epoxy-repaired specimens, the crack initiated at the notch and then propagated through the concrete, away from the interface. The epoxy-repaired specimens exhibited slightly higher ultimate strengths than the plain, notched specimens. These experiments provided calibration data for the Phase II models.
4. Five reinforced concrete beam experiments were conducted on “as-built” and epoxy-repaired specimens in order to provide simple validation data on the

system level. The epoxy-repaired specimens were loaded to induce cracking of various levels, unloaded, repaired with epoxy, and then reloaded to failure. In the cases where the cracks were very small (< 0.006 in), the epoxy did not have a significant effect on the ultimate capacity, but the beam behaved in a more brittle fashion. Interestingly, in the experiments where the cracks were larger (> 0.006 in), the epoxy-repaired beams exhibited a much higher capacity than the "as-built" structures. The failure mechanism and ductility of the beam were also affected. Because the repair significantly changed the overall behavior of the beam, it is recommended that additional research be conducted to understand the overall effect that using HWMM has on larger pre-stressed beams and, subsequently, the effect it has on the entire bridge structure including loads transferred to adjacent elements.

CHAPTER 6. REFERENCES

1. Alexander, M., & Mindess, S. (2014). *Aggregates in concrete*. CRC Press.
2. ASTM International. (2017). *ASTM C496/C496M-17 Standard Test Method for Splitting Tensile Strength of Cylindrical Concrete Specimens*.
3. ASTM International. (2018). *ASTM C39/C39M-18 Standard Test Method for Compressive Strength of Cylindrical Concrete Specimens*.
4. Bardella, L. (2001). A phenomenological constitutive law for the nonlinear viscoelastic behavior of epoxy resins in the glassy state. *Construction and Building Materials*, *21*(1), 157-163.
5. Bažant, Z. P. (1992). Fracture mechanics of concrete structures: part I, state-of-art report. *ACI Committee*, *446*.
6. Coronado, C. A., & Lopez, M. M. (2008). Experimental characterization of concrete-epoxy interfaces. *Journal of Materials in Civil Engineering*, *20*(4), 303-312.
7. Courard, L., Piotrowski, T., & Garbacz, A. (2014). Near-to-surface properties affecting bond strength in concrete repair. *Cement and Concrete Composites*, *46*, 73-80.
8. Czarnecki, S., & Hoła, J. (2016). Evaluation of the height 3D roughness parameters of concrete substrate and the adhesion to epoxy resin. *International Journal of Adhesion and Adhesives*, *67*, 3-13.
9. Gergely, P., & Sozen, M. A. (1967). *Design of anchorage-zone reinforcement in prestressed concrete beams* (No. 82). University of Illinois.
10. Georgia Department of Transportation. (2013). *Standard Specifications Construction of Transportation Systems*. Georgia Department of Transportation.
11. Guo, J. S., & Waldron, P. (2001). An elastic model to quantify the effect of moisture on the mechanical properties of concrete at the time of test. *Magazine of Concrete Research*, *53*(3), 151-162.
12. Hillerborg, A. (1985). The theoretical basis of a method to determine the fracture energyG F of concrete. *Materials and structures*, *18*(4), 291-296.
13. Issa, C. A., & Debs, P. (2007). Experimental study of epoxy repairing of cracks in concrete. *Construction and Building Materials*, *21*(1), 157-163.
14. Lee, J., & Lopez, M. M. (2014). An experimental study on fracture energy of plain concrete. *International Journal of Concrete Structures and Materials*, *8*(2), 129-139.
15. Li, G. (2004). *The effect of moisture content on the tensile strength properties of concrete* (Doctoral dissertation, University of Florida).
16. Monteiro, P. (2006). *Concrete: microstructure, properties, and materials*. McGraw-Hill Publishing.
17. Okada, K., KobayashiI, K., & Miyagawa, T. (1988). Influence of longitudinal cracking due to reinforcement corrosion on characteristics of reinforced concrete members. *ACI Structural Journal*, *85*(2).
18. PCI (2001). Bridge Member Repair Guidelines, Precast/Prestressed Concrete

Institute (PCI) Northeast Region, Technical Committee, Report no. PCINER-01-BMRG
19. Reinhardt, H. W., Rossi, P., & van Mier, J. G. (1990). Joint investigation of concrete at high rates of loading. *Materials and Structures*, *23*(3), 213-216.
20. Ross, C. A., Jerome, D. M., Tedesco, J. W., & Hughes, M. L. (1996). Moisture and strain rate effects on concrete strength. *Materials Journal*, *93*(3), 293-300.
21. Shin, H. C., Miyauchi, H., & Tanaka, K. (2011). An experimental study of fatigue resistance in epoxy injection for cracked mortar and concrete considering the temperature effect. *Construction and Building Materials*, *25*(3), 1316-1324.
22. Tadros, M. K., Badie, S. S., & Tuan, C. Y. (2010). *Evaluation and Repair Procedures for Precast/Prestressed Concrete Girders with Longitudinal Cracking in the Web* (Vol. 654). Transportation Research Board.
23. Transpo Industries. (2017). *Sealate T-70 Technical Data Sheet*.
24. Xu, H., & Arson, C. (2014). Anisotropic damage models for geomaterials: theoretical and numerical challenges. *International Journal of Computational Methods*, *11*(02), 1342007.
25. Xu, H., Busetti, S., & Arson, C. (2017). Fracture-induced anisotropy of the stress–strain response of shale at multiple scales. *International Journal of Geomechanics*, *17*(8), 04017036.

APPENDIX A STRUCTURAL DRAWINGS

6 5 4 3 2 1

Unreinforced 3 foot Beam: Notched

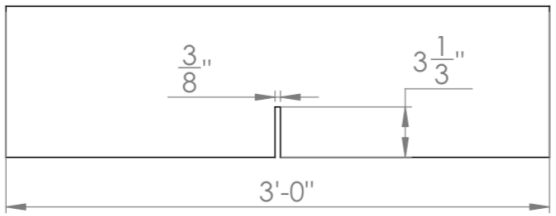

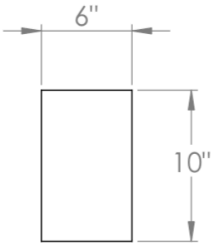

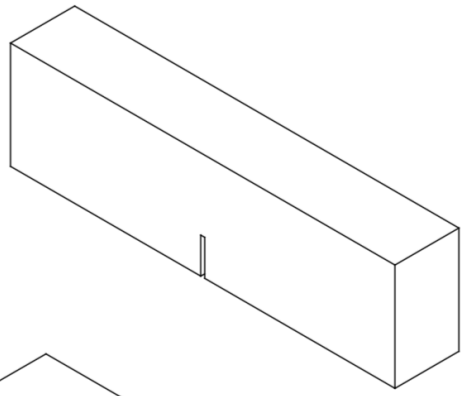

Unreinforced 3 foot Beam: Notched and Epoxy Repair

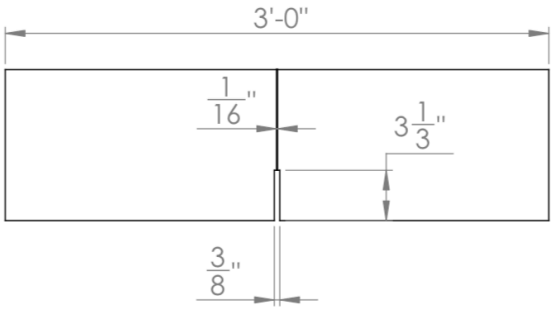

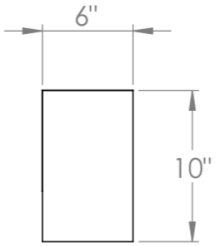

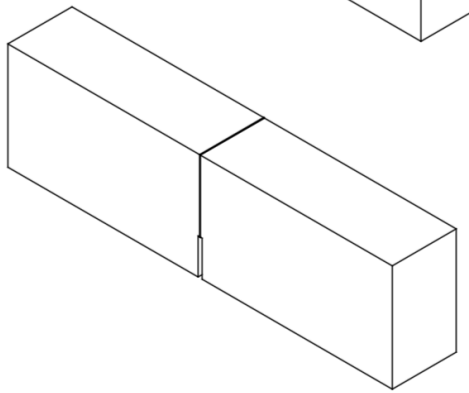

Notches occur at the midspan of the beam

UNLESS OTHERWISE SPECIFIED: DIMENSIONS ARE IN MILLIMETERS SURFACE FINISH: TOLERANCES: LINEAR: ANGULAR:		FINISH:			DEBURR AND BREAK SHARP EDGES	DO NOT SCALE DRAWING / REVISION
	NAME	SIGNATURE	DATE			TITLE: Unreinforced 3 foot Beams Notched Notched and Epoxy Repair
DRAWN	RLT		10/4			
CHK'D						
APPV'D						
MFG						
Q.A				MATERIAL: 5000 psi Concrete HMWMM epoxy		DWG NO. Unreinf. 3' Bms / A4
				WEIGHT:		SCALE:1:10 / SHEET 1 OF 1

6 5 4 3 2 1

Unreinforced 4 foot Beam: Notched

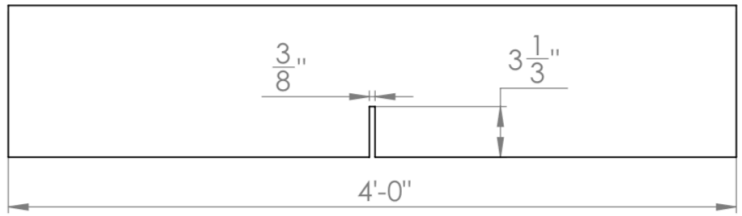

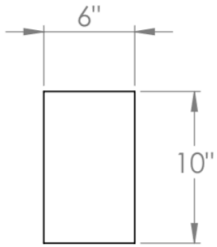

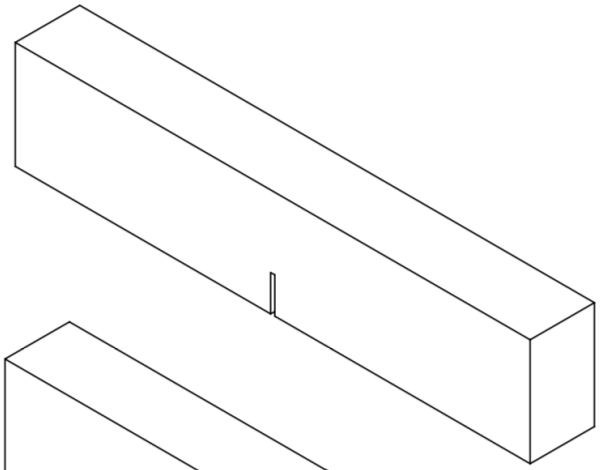

Unreinforced 4 foot Beam: Notched and Epoxy Repair

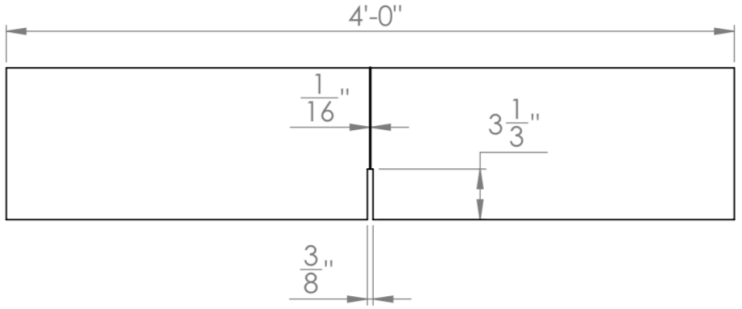

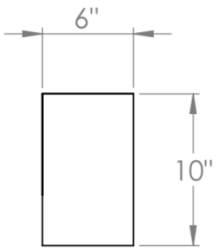

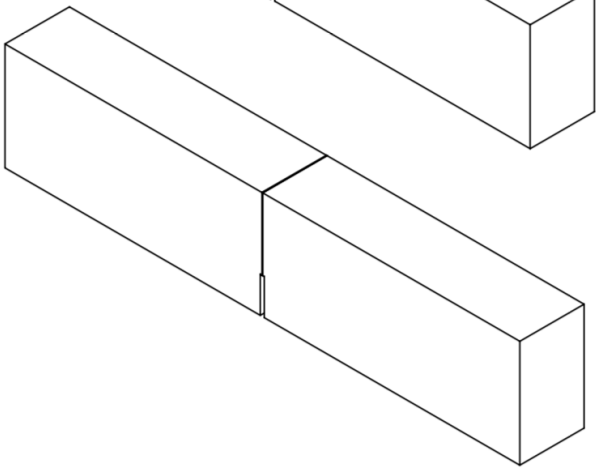

Notches occur at the midspan of the beam

UNLESS OTHERWISE SPECIFIED: DIMENSIONS ARE IN MILLIMETERS SURFACE FINISH: TOLERANCES: LINEAR: ANGULAR:		FINISH:		DEBURR AND BREAK SHARP EDGES	DO NOT SCALE DRAWING	REVISION
	NAME	SIGNATURE	DATE		TITLE: Unreinforced 4 foot Beams Notched Notched and Epoxy Repair	
DRAWN	RLT		10/4			
CHK'D						
APPV'D						
MFG						
Q.A				MATERIAL: 5000 psi Concrete HMWMM epoxy	DWG NO. Unreinf. 4' Bms	A4
				WEIGHT:	SCALE:1:10	SHEET 1 OF 2

Reinforced 4 foot Beam

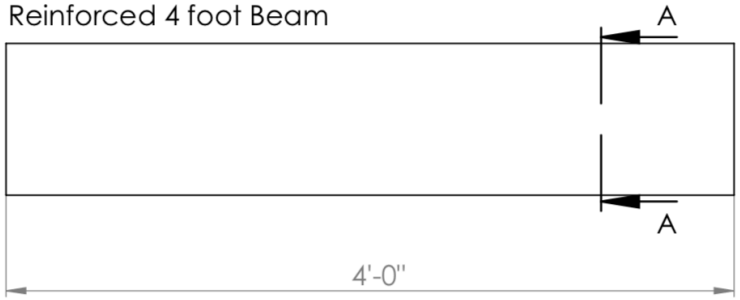

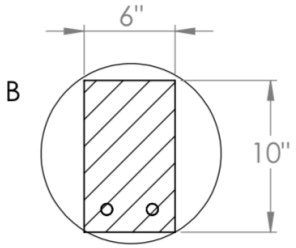

SECTION A-A

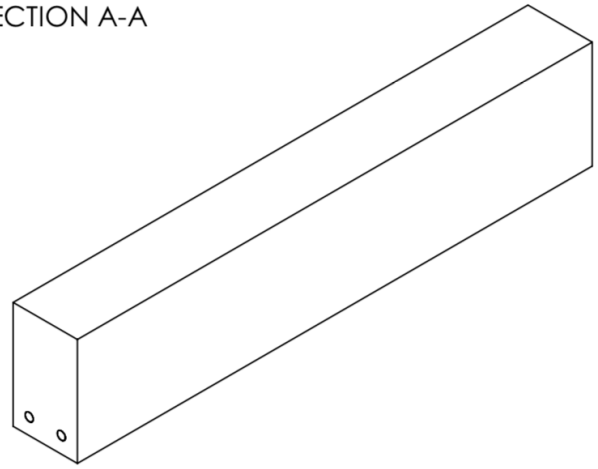

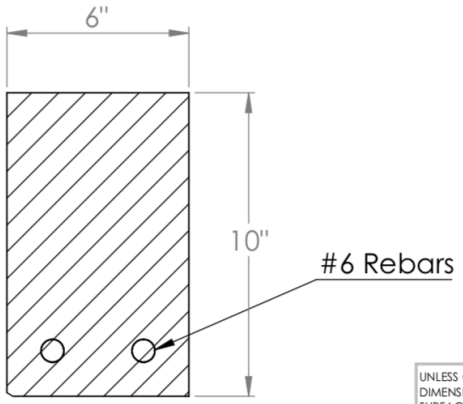

DETAIL B
SCALE 1 : 5

UNLESS OTHERWISE SPECIFIED: DIMENSIONS ARE IN MILLIMETERS SURFACE FINISH: TOLERANCES: LINEAR: ANGULAR:		FINISH:		DEBURR AND BREAK SHARP EDGES		DO NOT SCALE DRAWING	REVISION
	NAME	SIGNATURE	DATE			TITLE:	
DRAWN	RLT		10/4			Reinforced 4 foot Beams	
CHK'D							
APPV'D							
MFG							
Q.A				MATERIAL: 5000 psi Concrete HMWMM epoxy		DWG NO. Reinf. 4' Beams	A4
				WEIGHT:		SCALE:1:10	SHEET 1 OF 1

APPENDIX B MATERIALS

Thomas_Concrete,_Inc.
2500_Cumberland_Pky_S-200
Atlanta, Georgia 30339

DEPARTMENT OF TRANSPORTATION - HIGHWAY DIVISION
PORTLAND CEMENT CONCRETE MIX DESIGNS

Date: 3-16-18

CONCRETE PLANT: 737

PLANT LOCATION: Atlanta

MATERIALS		CODE	TYPE	SPGR	%ABS	F/F
Cement:	Holcim US, Inc. Holly Hill, SC	22	1	3.14		
Cement:	National Cement Co. of AL, Inc. Ragland,AL	41	1	3.14		
Sand Primary:	Vulcan Materials Co. Norcross,GA (10SM)	107F	2	2.69	0.30	
Stone:	Vulcan Materials Co. Norcross,GA	048	2	2.71	0.48	
Admixture:	Sika Corporation Plastiment Type D Lyndhurst,NJ.	14	1			
AEA:	Sika Corporation "SIKA AEA-14"					

CHECK MIX USED

ONE CUBIC YARD PROPORTIONS (SSD)

ONLY FOR USE ON DOT PROJECTS FOR EMERGENCY ROAD REPAIRS

1/11/2017

Class Concrete	24 HR ACCEL.							
Cement (lbs.)	752							
Sand -Primary (lbs.)	1045							
Stone (lbs.)	1893							
Water (gals.)	35.0							
Design Air (%)	4.0							
Accept. Air (LL-UL)	3.0 - 6.0							
Water Reducer (ozs.)	*. *							
Retarder (ozs.)	*. *							
Fine Agg Ratio (F/A)	0.36							
Stone Size	57							
Design Slump (ins.)	3.00							
Accept. Slump (LL-UL)	2.0 - 5.0							
Max. Water/Cu.Yd.	40.6							

737-4.1

LL=Lower Limit; UL=Upper Limit

* Retarder will be used when required by Specifications or placement conditions dictate it.

. Refer to temperature/dosage chart for retarder dosages.

The above concrete mix design proportions are for use on Department of Transportation projects. The ability of these proportions to produce concrete that meets specification requirements remains the responsibility of the Contractor. Jobsite acceptance of concrete produced with these proportions shall be based upon the Standard Specifications and SOP-10.

Concrete Engineer
or Certified Technician Jeff Duckworth

01/2017

Plant	: Atlanta		
Start Time	: 03/16/18 09:43:51	End Time	: 03/16/18 09:44:50
Product Code	: 508000	Destination	: Loadout
Load Size	: 3.00	Ticket	: 7365326
Truck No.	: 2742	Load Id	: 72010
Job	: 221	Customer	: GEORGIA TECH
Water Trim	: -2 gal	Moist. Water	: 18.99
Ideal W/C	: 0.3773	Acutal W/C	: 0.3545

MATERIAL	DESIGN	TARGET		ACTUAL		MST	ABS
TYPE I	752.00	2256.00	lb	2260.00	lb		
57 STONE	1858.00	5574.00	lb	5800.00	lb	0.00%	0.00%
MANUFACTURED SAN	1061.00	3336.74	lb	3440.00	lb	4.83%	0.00%
WATER	34.00	77.58	gal	77.00	gal		
AIR 14	7.20	21.60	floz	21.00	floz		
PLASTIMENT	11.30	33.90	floz	34.00	floz		

SCALE	START TARE	END TARE
AggLoadCell1	0 lb	5820 lb
AggLoadCell5	0 lb	3440 lb
CemLoadCell1	15 lb	2275 lb
WtrLoadCell1	0 gal	77 gal

CASTEK® INC.
A TRANSPO INDUSTRIES COMPANY

Technical Data Sheet

High Molecular Weight Methacrylate (HMWM) Crack Sealer
Sealate® (T-70-10 and T-70 MX-30)

Sealate® is a specially formulated, high molecular weight methacrylate resin system that is highly effective for sealing and filling cracks in concrete structures.

Application Procedure

Surface Preparation: It is strongly recommended that all concrete surfaces that are to receive Sealate® be thoroughly clean and sound. Remove all surface dirt, grease, paint, rust, and other contaminates by sand blasting or shot blasting. Applications on LMC overlays do not require blasting or mechanical abrasion, the surface can be high pressure washed to remove contamination. Before application of Sealate® the surface must be dry for 24 hours and just prior to application cracks should be cleaned with dry high pressure compressed air. The concrete surface should be visibly dry and the moisture content in the concrete should be tested according to ASTM D4263. The ambient temperature should be between 50ºF and 100ºF prior to resin application.

Mixing: Table 1 lists the mixing ratios of the two curing agents. Add the appropriate amount of Cobalt Napthenate promoter to Sealate® resin and mix well. Then add the corresponding amount of CHP initiator, stir again for approximately one to two minutes. If mechanically applied, the resin should be mixed utilizing a two component resin system using promoted resin for one part and initiated resin for the other part. Mixing ratio of promoted/initiated resin should be 1:1. The mixed resin should be applied to the concrete surface within five minutes of complete mixing.

Table 1: Mixing Instructions for Sealate®, Cobalt Napthenate and CHP

Sealate® (gal)	Cobalt Napthenate (mL)	CHP (mL)
1	75	150
5	375	750

CAUTION: Never mix CHP initiator with Cobalt promoter. A violent reaction will result!

Application: The rate of application of mixed resin should be approximately 100-150 square feet per gallon. However, this will vary depending on the surface, porosity, size, and quantity of cracks present in the area being treated.

During application, the concrete surface should be flooded with the resin, allowing sufficient time for penetration into the surface and complete filling of all cracks. Excess material should be redistributed using squeegees or brooms within 15 minutes after application. The quantity of initiated/promoted resin mixed at one time should be limited to five gallons.

Broadcasting of Aggregate: Broadcast sand should be applied to the entire treated area prior to cure, typically at 1-2 pounds per square yard. The sand used should be 12 x 16 mesh, #1 or #2 blasting sand, and should have a maximum moisture content no greater than 0.5%. It should be placed within 15 minutes of the resin application and before any setting of monomer occurs. Traffic can be restored once the concrete surface is cured tack-free. Refer to Table 2 for temperature restrictions and cure times.

Table 2: Cure Times for Sealate®

Ambient Temperature	Approximate Cure Time	
	T-70-10	T-70 MX-30
50°F – 70°F	7 – 12 hr	8 – 16 hr
70°F – 100°F	4 – 7 hr	5 – 8 hr

*Cure times are approximate and will vary with ambient and deck temperature, humidity, and sunlight. Structures can be opened to traffic only after complete cure is achieved.

TRANSPO INDUSTRIES, INC.
The Smart Solutions Company

ISO 9001 REGISTERED FIRM

Table 3: Properties* of Sealate®

Property	Results		Test Method
	T-70-10	T-70 MX-30	
Viscosity	15 – 25 cps (MPa-sec)	10 – 25 cps (MPa-sec)	ASTM D2395
Density	8.6 lb/gal (1.03 g/mL)	8.5 lb/gal (1.02 g/mL)	ASTM D1425
Gel Time/Pot Life @ 70ºF	35 – 40 min	50 – 60 min	AASHTO T237
Tack Free Time @ 70ºF	4 – 7 hr	5 – 8 hr	AASHTO T237
Solids Content	100%	100%	ASTM D1644
Tensile Strength	1,600 psi (>11.0 MPa)	>1,100 psi (>7.6 MPa)	ASTM D638 Type I
PCC-SSD Bond Strength	>615 psi (>4.2 MPa)	>615 psi (>4.2 MPa)	CA Test 551
Tensile Elongation	1 – 5%	>30%	ASTM D638 Type I
Volatile Content	30% max	40 – 45%	ASTM D2369
Slant Shear Bond Strength	>2,000 psi (>13.8 MPa)	>2,000 psi (>13.8 MPa)	ASTM C882
Vapor Pressure @ 77°F	0.62 mm Hg	0.52 mm Hg	ASTM D323 Reid Method

*To be used as general guidelines only

Packaging

Sealate® comes in one, five and fifty-five gallon containers. The initiator, Cumene Hydroperoxide (CHP) and the Cobalt Napthenate promoter are provided in separate labeled containers and in pre-measured quantities to make scale mixes of Sealate®.

Storage

Sealate® should be stored in tightly sealed containers in a dry location and at normal room temperatures (50ºF - 85ºF). The initiator, Cumene Hydroperoxide (CHP) and the Cobalt Napthenate promoter are provided in separate labeled containers, and should be stored in a cool shaded area separately from each other as well as away from the monomer.

Caution

Direct contact with Sealate® may produce minor skin irritations to persons prone to such reactions. It is recommended that all persons involved in mixing and application wear protective clothing such as goggles, rubber boots, and rubber gloves. As with all chemicals, read SDS prior to use.

Warranty

The following warranty is made in lieu of all other warranties, either expressed or implied. This product is manufactured of selected raw materials by skilled technicians. Neither seller nor manufacturer has any knowledge or control concerning the purchaser's use of product and no warranty is made as to the results of any use. The only obligation of either seller or manufacturer shall be to replace any quantity of this product that proves to be defective. Neither seller nor manufacturer assumes any liability for injury, loss or damage resulting from use of this product.

20 Jones Street, New Rochelle, NY 10801

Tel: 914-636-1000 Fax: 914-636-1282
Web: http://www.transpo.com Email: info@transpo.com